J. Fluid Mech. (1981), *vol.* 106, *pp.* 149–213
Printed in Great Britain

Energy flow in the cochlea

By JAMES LIGHTHILL
University College London

With moderate acoustic stimuli, measurements of basilar-membrane vibration (especially, those using a Mössbauer source attached to the membrane) demonstrate:

(i) a high degree of *asymmetry*, in that the response to a pure tone falls extremely sharply above the characteristic frequency, although much more gradually below it;

(ii) a substantial phase-lag in that response, and one which increases monotonically up to the characteristic frequency;

(iii) a response to a 'click' in the form of a delayed 'ringing' oscillation at the characteristic frequency, which persists for around 20 cycles.

This paper uses energy-flow considerations to identify which features in a mathematical model of cochlear mechanics are necessary if it is to reproduce these experimental findings.

The response (iii) demands a travelling-wave model which incorporates an only *lightly* damped resonance. Admittedly, waveguide systems including resonance are described in classical applied physics. However, a classical waveguide resonance *reflects* a travelling wave, thus converting it into a standing wave devoid of the substantial phase-lag (ii); and produces a *low-frequency* cutoff instead of the high-frequency cutoff (i).

By contrast, another general type of travelling-wave system with resonance has become known more recently; initially, in a quite different context (physics of the atmosphere). This is described as critical-layer resonance, or else (because the resonance absorbs energy) critical-layer absorption. It yields a *high-frequency* cutoff; but, above all, it is characterized by the properties of the energy flow velocity. This falls to zero very steeply as the point of resonance is approached; so that wave energy flow is retarded drastically, giving any light damping which is present an unlimited time in which to dissipate that energy.

Existing mathematical models of cochlear mechanics, whether using one-, two- or three-dimensional representations of cochlear geometry, are analysed from this standpoint. All are found to have been successful (if only light damping is incorporated, as (iii) requires) when and only when they incorporate critical-layer absorption. This resolves the paradox of why certain grossly unrealistic one-dimensional models can give a good prediction of cochlear response; it is because they incorporate the one essential feature of critical-layer absorption.

At any point in a physical system, the high-frequency limit of energy flow velocity is the slope of the graph of frequency against wavenumber† at that point. In the cochlea, this is a good approximation at frequencies above about 1 kHz; and, even at much lower frequencies, remains good for wavenumbers above about 0·2 mm^{-1} (which excludes only a relatively unimportant region near the base).

Frequency of vibration at any point can vary with wavenumber either because

† In any travelling wave, the wavenumber is the rate of change of phase with distance; for example, it is $2\pi/\lambda$ in a sine wave of length λ.

stiffness or inertia varies with wavenumber. However, we find that models incorporating a wavenumber-dependent membrane stiffness must be abandoned because they fail to give critical-layer absorption; this is why their predictions (when realistically light damping is used) have been unsuccessful. Similarly, models neglecting the inertia of the cochlear partition must be rejected.

One-dimensional modelling becomes physically unrealistic for wavenumbers above about 0·7 mm^{-1}, and the error increases with wavenumber. The main trouble is that a one-dimensional theory makes the effective inertia 'flatten out' to its limiting value (inertia of the cochlear partition alone) *too rapidly* as wavenumber increases. Fortunately, a two-dimensional, or even a three-dimensional, model can readily be used to calculate a more realistic, and significantly more gradual, 'flattening out' of this inertia. All of the models give a fair representation of the experimental data, because they all predict critical-layer absorption. However, the more realistic two- or three-dimensional models must be preferred. These retard the wave energy flow still more, thus facilitating its absorption by even a very modest level of damping. The paper indicates many other features of these models.

The analysis described above is preceded by a discussion of waves generated at the oval window. They necessarily include:

(*a*) the already-mentioned travelling wave, or 'slow wave', in which the speed of energy flow falls from around 100 m s^{-1} at the base to zero at the position of resonance;

(*b*) a pure sound wave, or 'fast wave', travelling at 1400 m s^{-1}, with reflection at the apex which makes it into a standing wave. Half of the rate of working of the stapes footplate against the oval window is communicated as an energy flow at this much higher speed down the scala vestibuli, across the cochlear partition and back up the scala tympani to the round window, whence it becomes part of the slow general apical progress of the travelling wave; a progress which, as described above, comes to a halt altogether just in front of the position of resonance.

Mathematical detail is avoided in the discussion of cochlear energy flow in the main part of the paper (§§ 1–10), but a variety of relevant mathematical analysis is given in appendices A–E. These include, also, new comments about the functions of the tunnel of Corti (appendix A) and the helicotrema (appendix C).

---

1. Introduction

This paper is an attempt to review the literature concerned with the mechanical response of the cochlea to stimuli low enough in amplitude for that response to be linear. Both the experimental data (Békésy 1960; Johnstone, Taylor & Boyle 1970; Rhode 1971, 1973; Kohllöffel 1972, 1973; Wilson & Johnstone 1975; Robles, Rhode & Geisler 1976; Gunderson, Skarstein & Sikkeland 1978) and the mathematical models (Zwislocki 1948, 1965; Ranke 1950; Peterson & Bogert 1950; Bogert 1950; Fletcher 1951; Lesser & Berkley 1972; Berkley & Lesser 1973; Schroeder 1973; Steele 1974, 1976; Steele & Taber 1979*a*, *b*; Siebert 1974; Zweig 1976; Zweig, Lipes & Pierce 1976; Geisler 1976; Cole & Chadwick 1977; Allen 1977; de Boer 1979; Viergever 1980) are discussed from the unifying standpoint of energy-flow considerations. On the other hand, there is almost no reference to:

(i) mechanics of the middle ear (except for its interaction with questions of cochlear input impedance);

(ii) those nonlinear effects which are observed to modify cochlear response at very high stimulus levels and, also, are presumed responsible for the enigmatic properties of combination tones;

(iii) the role of the hair cells is transduction of the cochlea's mechanical response into neural activity;

(iv) the neurophysiology of hearing.

Cochlear mechanics is, of course, important as providing a 'first filter' in the frequency-analysing function of the auditory system. The personal work of three decades summarized in the book of Békésy (1960) first gave clear experimental proof of this. See, for example, the graphs on page 454, which plot vibrational amplitudes as a function of frequency for six positions along the cochlear partition, as measured by Békésy in a human cadaver at extremely high stimulus levels. They show a fairly sharp maximum response at the characteristic frequency of each position.

Nevertheless, Békésy realized that the sharpness he measured was insufficient to explain the ear's accuracy in frequency discrimination, and he postulated a neurophysiological 'sharpening up' process. When Békésy's only moderately sharp tuning curves were compared later with the enormously sharper tuning curves of auditory nerve fibres as measured by Kiang *et al.* (1965), the need to postulate a 'second filter' operating either at the transduction stage or at the neurological stage became universally accepted.

Still more recent evidence, however, while generally supporting the need for a second filter, has tended to re-emphasize, and to strengthen belief in, the great importance of the first filter provided by the cochlea's mechanical response. The principal evidence came from two new experimental methods, using (*a*) the Mössbauer technique (Johnstone *et al.* 1970; Rhode 1971, 1973) and (*b*) laser-light fuzziness detection (Kohllöffel 1972, 1973). Both allowed the measurement of basilar-membrane vibration *in vivo* at stimulus levels moderate enough to minimize nonlinear modifications of the response curve.

Under these conditions, the measured response curve fell off extremely sharply *above* the characteristic frequency, although much more gradually below it. Such asymmetry is also a prominent feature of tuning curves for auditory nerve fibres, as was re-emphasized in the measurements of Evans & Wilson (1973) and Kiang & Moxon (1974). Indeed, the combined data suggest that this important phenomenon (the large difference in steepness of tuning curves above and below the characteristic frequency) is due mainly to the cochlear-mechanics first-filter effect. It would then be sufficient to assume that a second filter, which recent work of Fettiplace & Crawford (1978) suggests may reside in the hair cells themselves (at least for frequencies less than about 1 kHz), generates a largely symmetrical further sharpening of response, relatively more modest in significance.

On this interpretation, the special psychophysical importance of the mechanics of the cochlea derives from the extremely sharp fall-off of auditory response curves which it produces *above* the characteristic frequency. This type of mechanical response, besides being important psychophysically, is also interesting from the point of view of mechanics. It is not surprising, then, that the increasingly precise data available on basilar-membrane response have stimulated experts in the mechanics of interacting motions of fluids and solids to aim at increasingly precise descriptions of cochlear mechanics.

Earlier, the work of Békésy had stimulated the development of some interesting mathematical models, starting with the work of Zwislocki (1948) and Ranke (1950). The most impressive of these (Peterson & Bogert 1950) went far towards *predicting* the extraordinary steepness of the tuning curve's high-frequency side under linear-response conditions, which was to be experimentally demonstrated two decades later by Rhode (1971) and others. This steepness, in fact, is clearly visible in Peterson & Bogert's figure 20, for a limiting case of zero damping, and would have been preserved after the incorporation of a *small* amount of damping. However, those authors preferred to put all their emphasis on conclusions for a model with rather large damping (Bogert 1950) because they were seeking agreement with the blunt tuning curves that Békésy (albeit at extremely high stimulus levels, for which large nonlinear effects are known to be present) had obtained.

Later, when the new experimental techniques allowing measurements of basilar-membrane vibration at moderate stimulus levels had demonstrated the enormously steep slope of the tuning curve above the characteristic frequency (a slope measured already by Johnstone *et al.* (1970), for example, as 95 dB/octave for the guinea pig cochlea), this striking characteristic of cochlear mechanics stimulated the construction of many new mathematical models. They included ingenious developments (Schroeder 1973; Zweig 1976) from the one-dimensional models pioneered by Zwislocki (1948), Peterson & Bogert (1950) and Fletcher (1951); that is, models in which changes of pressure are taken as uniform within each cross-section of the scala vestibuli (and, similarly, within each cross-section of the scala tympani).

At the same time, the two-dimensional type of model pioneered by Ranke (1950), which allows fluid disturbances in a scala cross-section to vary with distance from the cochlear partition, was developed much further by Lesser & Berkley (1972), Siebert (1974) and Allen (1977). Furthermore, this increase in the realism of the models was taken still further in the three-dimensional models of Steele (1974, 1976) which allowed for disturbances in the fluid to vary also across the *width* of the cochlear partition. One general conclusion from the two- and three-dimensional models was that, although the fluid disturbances must indeed be effectively one-dimensional near the base, they cannot be even approximately one-dimensional near the position of maximum disturbance.

The different models are discussed in this paper from two points of view. One of these is to analyse what features a model needs if it is to show the sharp asymmetry of amplitude distribution and monotonicity of phase distribution characteristic of all the refined measurements of basilar-membrane vibration. This analysis is used to explain why the features in question, obviously essential to a satisfactory model, are present in some (but not all) one-dimensional models as well as in some (but not all) two- and three-dimensional models.

Besides applying, as it were, such a 'first filter' to the available models, the paper goes on to apply a 'second filter'; this discriminates among all those different models that lead to broadly correct types of amplitude and phase distribution by giving preference to those with the most physically realistic assumptions. The discussion here reinforces conclusions by Steele (1976) that a three-dimensional model's clear advantage from this point of view outweighs the only moderately greater complexity in analysis which it need entail. The discussion includes also a critical review of the very various assumptions by different authors regarding the distribution of the coch-

lear partition's stiffness and inertia. In addition, it points out, as did Geisler (1976), that it is undesirable to neglect either the compressibility of the cochlear fluids, which can affect response at very high frequencies, or the fluid mechanics of the helicotrema, which is significant at very low frequencies. Methods of properly taking these into account were indicated by Peterson & Bogert (1950) and by Fletcher (1951), respectively, and are developed further in this paper.

2. Significance of the cross-sectional mean pressure

The analysis starts, in fact, by considering a separation of the pressure distribution within a cochlear cross-section into (i) its *mean value, P, over the cross-section's area* (on both sides of the cochlear partition), and (ii) its *deviation from the mean, p* (taking opposite signs on the partition's two sides). For the details of this analysis, see appendix A. It is the distribution of p (a generalization of Peterson & Bogert's p_-) which is analysed by most model-builders and takes the well-known travelling-wave form, with phase decreasing from base to apex.

By contrast, P is a generalization of Peterson & Bogert's p_+ and may be rather accurately given by their calculation as an *acoustic standing wave*. Its presence may need to be taken into account in interpreting certain data; and, in particular, the observation that the high-frequency limit of phase was always an integer multiple of π in the experiments of Rhode (1971). Such behaviour is inconceivable in a travelling-wave system.

Physically, the standing wave is generated as a combination of a sound wave travelling from base to apex and its reflection (a sound wave travelling from apex to base). The combined wave involves motions which are in phase at all points of the cochlea.

Thus, the main travelling-wave distribution of pressure deviations from the mean, p, is necessarily accompanied by a more modest standing-wave distribution of cross-sectional mean pressures P, all vibrating in phase with the motion of the stapes. It is possible (see appendix A for details) that these can generate a small in-phase motion of the cochlear partition as a whole (including the basilar membrane) which Rhode picked up at the measurement site as the leading signal for frequencies above the characteristic frequency. These are frequencies at which the energy in the main travelling wave is absorbed before the measurement site is reached. In that case, the monotonic change in phase characteristic of a travelling wave would continue to be measured until (as the characteristic frequency was exceeded) the travelling wave was suppressed in favour of the in-phase standing-wave behaviour generated in the cochlea as a whole by the mean pressure P. The method of inferring phase from the measure-meants would then reckon it to make a transition to a neighbouring multiple of π corresponding to an in-phase motion.

A second interesting feature of the standing-wave behaviour of the cross-sectional mean pressure P is Peterson & Bogert's prediction of a resonant acoustic response of the whole cochlea in this mode at a particular high frequency around 12 kHz. That may need to be borne in mind in any discussions of cochlear damage by high-frequency sound.† However, this paper's main concern with the distribution of cross-sectional mean pressure P is in the context of energy flow.

† See appendix A for discussion of a possible function of the tunnel of Corti in damping this resonance.

The best-known feature of energy flow in the cochlea is that energy *travels* (that is, moves in the form of a 'travelling wave') from the base towards the apex, but becomes dissipated before reaching the apex except at low frequencies (below about 300 Hz). The energy in question takes two forms: potential energy associated with the elastic properties of the cochlear partition, and kinetic energy associated with the inertia of the cochlear partition and of the fluid motion outside it. Chapters 11 and 12 of Békésy (1960) amass a large amount of evidence for this travelling-wave interpretation of cochlear mechanics, and the newer measurements at moderate stimulus levels such as those of Rhode (1971) have put the matter beyond any doubt; especially, through their demonstration that the phase of basilar-membrane vibration at a fixed point varies monotonically as the frequency increases up to its characteristic value.

On the other hand, the fact that a significant fraction of the total energy in the travelling wave consists of the kinetic energy of the fluid in the scala tympani appears to raise problems; essentially, because the only power source (the rate of working by the stapes footplate against the oval window) acts exclusively on the fluid in the scala vestibuli. Only a consideration of how the cross-sectional mean pressure P propagates at the speed of sound can explain how a part of that rate of working is communicated at this very high speed down part of the scala vestibuli, across the cochlear partition and back up the scala tympani to the round window, whence the energy flow can become part of the slow general apical progress of the travelling wave (appendix A).

Related considerations resolve the apparent paradox in the experiments reported by Wever & Lawrence (1954) on page 275. They found, in a cat's cochlea, very similar disturbance patterns (as estimated by the distributions of cochlear potentials) whether it was acoustically stimulated at the *base* or at the *apex*. They questioned whether this was consistent with the idea of a wave travelling from base to apex and being dissipated *en route*. Analysis in appendix A shows, however, why with apical stimulation the energy travels (carrying a distribution of cross-sectional mean pressure P) at the speed of sound from apex to base, where (because of the differing impedances of the round and oval windows) it sets up a slow, apically travelling wave of deviations p from that cross-sectional mean.

Another, similar question treated briefly in appendix A is concerned with those familiar, and rather modest, alterations in cochlear disturbance patterns that occur when the scala tympani has been drained. Apart from the present section and appendix A, however, the rest of the paper deals with the classical subject matter of cochlear mechanics: the main travelling wave carrying pressure deviations p from the cross-sectional mean.

3. Travelling-wave models and resonance

Békésy (1960) tended to draw a sharp distinction between his 'travelling-wave' interpretation of cochlear mechanics and any possible 'resonance' theory. It is, of course, true that no simple resonating system with one degree of freedom (such as Helmholtz originally proposed) could show even the limited asymmetry of frequency response which Békésy himself found, let alone the extremely one-sided steepness of response reduction (that is, steepness above, but not below, the characteristic frequency) found at moderate stimulus levels.

Huxley (1969) pointed out, however, that a *combination* of a travelling-wave system

and a resonant system is conceivable; in such a system, a travelling wave would carry energy along to the position of resonance, where it would remain in a local oscillation until it were damped. He proposed, as a practical test of whether resonance in this sense was acting (essentially, to limit the travel of the wave) the criterion: do we observe that 'incoming energy is stored over a considerable number of cycles in a mechanically oscillating structure'?

A clear affirmative answer to this question was given by the experiments of Robles *et al.* (1976). They used the Mössbauer technique to measure the response of the basilar membrane of a squirrel monkey *in vivo* to acoustic clicks 0·15 ms in duration. After the expected delay (time required for the travelling wave to reach the observation site) the basilar membrane's response was oscillatory with a period near that of its characteristic frequency; and it did indeed continue for 'a considerable number of cycles' (typically, 15–25).

These results are consistent with the idea that damping is relatively light. They suggest, indeed, that a mathematical model for cochlear mechanics should be rejected if it can achieve good prediction of characteristic frequencies only by assuming large damping coefficients. Rather, there is a need for mathematical models which combine travelling-wave features and resonance features and which predict, even with quite small damping, the necessary sharp fall-off of amplitude above the characteristic frequency.

Wave physics distinguishes between two main types of lightly damped travelling-wave systems which exhibit resonance (at a different frequency for each point). Of these two types, one is much more widely familiar to physicists because it is extremely *commonly* found; especially, in waveguides of all kinds. We shall call this first type of resonance in a travelling-wave system 'classical waveguide resonance'. It is characterized by three main properties, as follows:

(i) at each point, the frequency for which resonance occurs is a *low-frequency* cutoff; that is, no wave energy at frequencies below the resonant frequency can pass the point;

(ii) as a travelling wave of fixed frequency ω approaches the point where the resonant frequency is ω, its *wavelength increases*, although the speed of travel of the wave energy is gradually reduced;

(iii) nevertheless, wave energy at frequency ω reaches the point where the resonant frequency is ω after a finite time, when it is immediately *reflected*.

Although the cochlea is certainly a waveguide, we see that it is not a 'classical waveguide' of the type exhibiting this kind of resonance. Indeed, it has properties opposite to (i), (ii) and (iii): the characteristic frequency at a point is a *high-frequency* cutoff; furthermore, as a wave of frequency ω approaches the point whose characteristic frequency is ω, its wavelength *decreases*; and, finally, the possibility of significant wave energy undergoing reflection from that point (which would make the wave more of a standing wave than a travelling wave) is ruled out by the phase measurements.† For example, Rhode (1971) found large phase lags (around 7π or more) of basilar-membrane displacement behind stapes displacement at the characteristic frequency.

† In this connection it should be noted that the experiments demonstrating high resonance peaks at moderate stimulus levels suggest light damping, which in the moderate time required for reflection according to (iii) above would imply small energy loss before reflection.

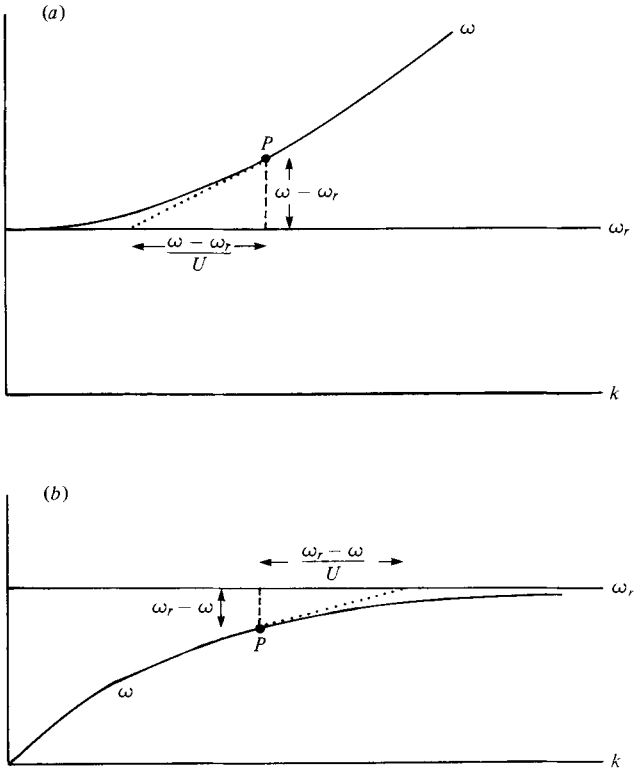

FIGURE 1. (*a*) Plot of radian frequency ω against wavenumber k, exhibiting low-frequency cut-off at a resonant frequency ω_r (as in classical waveguide resonance). The plot's necessarily positive slope U at a point P is the wave's 'group velocity' (speed at which it transmits energy) for the corresponding frequency and wavenumber. The perpendicular (broken line) dropped from P on to the line $\omega = \omega_r$ is of length $\omega - \omega_r$. The tangent at P (dotted line), with slope U, intersects the line $\omega = \omega_r$ at a distance $(\omega - \omega_r)/U$ from the foot of that perpendicular. Evidently, this distance decreases to zero as P moves along the curve to the left. Thus, although *both* $\omega - \omega_r$ *and* the slope U become smaller as P moves towards $k = 0$, they do so in such a way that the ratio $(\omega - \omega_r)/U$ decreases to zero. We can say, then, that U tends to zero much more gradually than $\omega - \omega_r$ itself. (*b*) Frequency–wavenumber plot with high-frequency cutoff at a resonant frequency ω_r (as in critical-layer absorption). The perpendicular (broken line) dropped from P on to the line $\omega = \omega_r$ is now of length $\omega_r - \omega$. The tangent at P (dotted line) with positive slope U intersects the line $\omega = \omega_r$ at a distance $(\omega_r - \omega)/U$ from the foot of that perpendicular. This distance increases indefinitely as P moves along the curve to the right (see appendix B for a demonstration of this for any dispersion relationship of the algebraic kind that necessarily results from physical properties described by differential equations). It follows that U tends to zero much more rapidly than $\omega_r - \omega$ itself.

4. Critical-layer absorption

The more recently discovered type of resonance in a travelling-wave system (Booker & Bretherton 1967) is called 'critical-layer resonance' or else (because the resonance absorbs energy) 'critical-layer absorption'. It is characterized by three main properties, as follows:

(i) at each point, the frequency for which resonance occurs is such that no wave energy at frequencies *above* it can pass the point;

(ii) as waves of that frequency approach the point, their wavelength *decreases* towards zero, while the speed of travel of their wave energy is *rapidly* reduced;

(iii) this reduction of travel speed with distance from the point is so rapid that the wave energy would require infinite time to reach that point; accordingly, no possibility of reflection can arise and any damping rate however light will remove all of that energy before it reaches the point.

It is important to note that properties (i), (ii) and (iii) all go together, being essentially consequences of one another, in critical-layer absorption; *and* that the same is true of the corresponding properties (i), (ii) and (iii) for classical waveguide resonance described in § 3. These logical relationships are most clearly intelligible from the classical law that wave energy travels, not at the speed of individual crests, but at a different speed called the *group velocity*, whose value can be determined from a frequency–wavenumber plot.

Here, the 'wavenumber' k is defined in a travelling wave as the rate of change of phase (in radians) with distance of travel. For example, when Rhode (1971) measured phase at two points on the squirrel-monkey basilar membrane at a distance 1·5 mm apart, he obtained data which can be used (see appendix B) to estimate the wavenumber (rate of decrease of phase with distance) between those points. Of course in a sinusoidal wave of wavelength λ we have $k = 2\pi/\lambda$ since the phase changes by 2π per wavelength; but our definition specifies k for much more general, non-sinusoidal waves in terms of their phase gradient.

Similarly, we use a radian frequency ω (in radians per second) which is 2π times the ordinary frequency in hertz (cycles per second). On a plot of ω against the wavenumber k observed for waves of that frequency at a given point, the group velocity U at that point is given by the *slope* (that is, gradient) of the curve. This slope must be positive (making ω an increasing function of k) if energy is to travel in the direction of decreasing phase.

Accordingly, for classical waveguide resonance (§ 3), property (i) implies a frequency–wavenumber plot like figure 1(*a*). In other words, with low-frequency cutoff at the resonant frequency ω_r, a frequency–wavenumber plot of positive slope must increase from the value $\omega = \omega_r$ at the *lowest* value of wavenumber (property (ii)); namely, $k = 0$ (for which the associated *wavelength* becomes large). Thus, the excess $(\omega - \omega_r)$ of wave frequency ω over the resonant frequency ω_r tends to zero as $k \to 0$. It commonly happens that the *slope* U of the curve in such a case also tends to zero, but if so it can only tend to zero much more *gradually* than $(\omega - \omega_r)$ itself. It is this property of the slope (that is, of the group velocity U at which the energy propagates) that allows energy of fixed frequency ω to reach the point where $\omega_r = \omega$ in a finite time (property (iii))... . Such a point is known in classical waveguide theory as a 'turning point', and a special type of mathematical representation of the amplitude distribution (based on the 'Airy function') is used to describe behaviour near a turning point.

By contrast, with critical-layer absorption as described in this section, property (i) implies a frequency–wavenumber plot like figure 1(*b*); thus, with high-frequency cutoff at the resonant frequency ω_r, a frequency–wavenumber plot of positive slope must rise up to the value $\omega = \omega_r$ as k increases to indefinitely large values (property (ii)). The frequency *defect* $(\omega_r - \omega)$ then tends to zero as k becomes large. This requires, however, that the slope U tends to zero much *more* rapidly than $(\omega_r - \omega)$ itself. This

property of the velocity at which the energy propagates means that energy of fixed frequency would require infinite time to reach the point where $\omega_r = \omega$ (property (iii)).

For fuller developments of these arguments, see appendix B. To sum them up, there is a sharp division between the two ways in which resonance may occur within a lightly damped travelling-wave system. For a mathematical model of the cochlea, *none* of the three basic properties of a classical waveguide resonance would be acceptable (and, in fact, each implies the other two). By contrast, *all* three basic properties of a critical-layer absorption (which, again, are logical consequences of one another) correspond well with the observations.

It is necessary, then, to reject mathematical models, however ingenious, which lead to a turning-point analysis typical of classical waveguide resonance. For example, the models of Cole & Chadwick (1977) based on a tapered-elastic-plate representation of the basilar membrane can be quickly seen to be unacceptable on these grounds; perhaps most quickly of all, by noticing that the solution's representation involves the Airy function; or else, more physically, by noticing that it exhibits all the three properties listed above. In particular, their solution (2–3) involves standing waves rather than travelling waves. Indeed, both this and the other two properties are well illustrated in the experiments on an associated physical model given in their figure 7, which shows the wavelength increasing (wavenumber decreasing) as resonance is approached; and, also, demonstrates that no waves of frequencies below the resonant frequency at a point can reach that point.

It may also be noted that, in the paper where Steele (1974) developed the first truly three-dimensional models of the cochlea (his models 1 and 2), he preceded his account of these by describing a crude model which he called 'model zero'. Steele's model zero, however, must be rejected as completely unacceptable because it too leads to a turning-point representation characteristic of classical waveguide resonance.

By contrast, the necessary feature, here called critical-layer absorption, is exhibited in quite a substantial group of models. This includes representatives of one-, two- and three-dimensional models.

5. One-dimensional models without resonance

In a one-dimensional model each cross-section of the cochlea has p (the pressure *deviation* from its mean value P over the cross-section) taking a uniform value right across the scala vestibuli; and another uniform value of opposite sign right across the scala tympani. That difference of pressure then produces a movement of the cochlear partition determined by its stiffness and inertia (together with any damping which the model may include).

All analyses suggest that, near the base of the cochlea, the stiffness is so large that it dominates over other mechanical properties of the partition (inertia and damping); and, also, that it forces the local pressure distribution near the base to be one-dimensional. In fact, a very early one-dimensional model of the cochlea (Zwislocki 1948) was stiffness-dominated. Consequentially, this model remains of great value in a region close to the base. Admittedly, the extent of that region becomes less as the frequency increases. On the other hand, at relatively low frequencies, the Zwislocki model is shown in appendix C to be especially helpful for suggesting how the cochlear

impedance to the motions of the stapes footplate is reduced (as frequency falls) from the typically well-matched value that it takes around 1 kHz or more.

Equally, as Steele & Taber (1979*a*, *b*) pointed out, the Zwislocki model at low frequencies exhibits an important change of character with respect to energy flow. At these frequencies, in fact, a travelling wave's essential characteristic (that fluid flow is in phase with excess pressure, giving one-way energy flow) is violated very near the base. Substantial components of fluid motion in quadrature with excess pressure are, indeed, necessarily present in that very limited 'near-field' region. Locally, these give the motion characteristics intermediate between a travelling wave and a standing wave (appendix C).

Beyond that limited region, however, the motion takes a pure travelling-wave form which, as Steele & Taber (1979*a*, *b*) emphasize, closely satisfies the convenient approximate rules that mathematicians and physicists call WKB. Physically, these mean that at each point energy travels at the above-mentioned group velocity (slope of the frequency–wavenumber plot calculated from the *local* properties of the system). Steele and Taber go on to show that the above-mentioned small 'near-field' region close to the base (which is only present at all for frequencies below about 1 kHz) is actually the only cochlear region where the WKB approximation is inappropriate. By contrast, those regions (farther from the base) where higher-dimensional models are required for good accuracy turn out to satisfy the WKB approximation rather closely. This is fortunate because three-dimensional models, in particular, would be difficult to implement if the WKB approximation were unavailable. It is also fortunate that, in the one limited region where the WKB approximation cannot be used, the motions are necessarily one-dimensional and can be readily described by the Zwislocki model (appendix C).

This model may also be a useful representation of the response of the *whole* cochlea to frequencies so extremely low that basilar-membrane vibration remains substantial all the way to the helicotrema. These are frequencies for which no true resonance occurs at any point. At these frequencies, a 'boundary condition' on p is needed to represent the fluid mechanics of the helicotrema. This application of the Zwislocki model is given in appendix C, which indicates how a transition from a travelling-wave to a standing-wave type of vibration, with the possibility of a rather special type of resonance, may occur as the frequency falls to these very low values.

At all higher frequencies than those, however, the Zwislocki model fails as a model of the cochlea as a whole. In fact, *at any given point* of the cochlea, it is useful only for frequencies well below the characteristic frequency. To see this, note that the model involves no possibility of any resonance being available to define such a characteristic frequency, although our earlier discussion suggested that the data can be explained only in terms of a lightly damped resonant system. A still more direct conflict with the data is that at each point the Zwislocki model makes the frequency–wavenumber plot a straight line through the origin. In other words, the model exhibits none of the 'dispersion' (wave velocity and group velocity varying with wavenumber) shown in more than one way to be present (appendix B) from the data of Rhode (1971) and others.

In fact, Zwislocki's model involves no possibility of normal cochlear-partition resonance because it allows no *inertial* component in the response of the cochlear partition. Under these circumstances, Zwislocki was able to calculate reasonable

values of characteristic frequency only by assuming large damping. This led to a broad frequency response above as well as below the characteristic frequency. Such a feature could still be defended much later by Zwislocki (1965) as compatible with the data, but can no longer be so defended.

6. One-dimensional models with resonance

Peterson & Bogert (1950) first produced a one-dimensional travelling-wave model of the cochlea which was able to admit resonance, by supposing the response of the cochlear partition to include an inertial component. Accordingly, their model was the first to demonstrate critical-layer absorption. In consequence (as noted in § 1 above) it foreshadowed the true asymmetry of frequency response (with a steep fall above, but not below, the characteristic frequency) two decades before it was observed.

Peterson & Bogert (1950) were also innovative in their treatment of the cochlear partition's stiffness. The type of stiffness which needs to be incorporated in all one-dimensional (and most other) models of the cochlea can be described as a volumetric stiffness; defined as the ratio

$$\frac{\text{pressure difference across the cochlear partition}}{\text{resulting volume displacement of the partition per unit length}}. \tag{1}$$

Rather naturally, Zwislocki (1948) used for his model the *direct* measurements of this quantity which Békésy (1941) had made and which are reproduced in Békésy (1960), figure 11–73. These measurements of volumetric stiffness vary by just *two* orders of magnitude along the length of the cochlea.

The existence of these volumetric stiffness data (even though, as we shall see, Békésy's method of measurement is seriously unsatisfactory in two important ways) has always been one of the main embarrassments facing a resonance interpretation of cochlear mechanics, for two reasons. First, only a much more modest variation in the corresponding inertia can be reasonably expected. If so, then the resonant frequency ω_r, with its classic form

$$\left(\frac{\text{stiffness}}{\text{inertia}}\right)^{\frac{1}{2}}, \tag{2}$$

could hardly vary by more than *one* order of magnitude along the length of the cochlea. This would be insufficient to explain data suggesting that characteristic frequencies vary by about *two* orders of magnitude.

By contrast, in a model like Zwislocki's that allows a travelling wave to reach its peak where stiffness and a large uniform *damping* are locally balanced, the characteristic frequency should vary along the cochlea by about the same factor as the stiffness itself (not its square root). In fact, the data derived by Greenwood (1961), on characteristic frequency in the six mammalian species on which Békésy had used his method of measuring volumetric stiffness, support rather well this prediction of direct proportionality. A few years later, therefore, Zwislocki (1965) could still claim that his type of model gave the best account of the available data.

To justify the rejection of this type of model in favour of a lightly damped travelling-wave model with resonance, then, we must not only point to the more recent measurements of basilar-membrane vibration as excluding models with heavy damping, but

give also clear reasons for accepting the results of these recent measurements while rejecting the volumetric-stiffness measurements of Békésy (1941). In fact, we are influenced to accept the results of Rhode (1971), for example, by the many checks on the internal consistency of those results which have been made by Zweig (1976); also, some more checks are made in appendix B; finally, the same technique used in other laboratories like that of Gunderson *et al.* (1978) led to closely comparable results. By contrast, the method of measuring volumetric stiffness used by Békésy (1941) gave results which are in conflict with later data which he himself obtained by a different method (Békésy 1947).

The method by which these later data, reproduced by Békésy (1960), pp. 466–9, were acquired now seems more reliable because local elastic properties of the basilar membrane itself were measured. A known force was applied at various points of the membrane by means of a fine hair, and the resulting local depth of depression determined microscopically. Peterson & Bogert (1950) already relied entirely on these measurements to estimate the stiffness of the cochlear partition, which Békésy had found to be dominated by that of the basilar membrane. They inferred, as also did Fletcher (1951), a stiffness varying by at least *three* orders of magnitude along the length of the cochlea.† For a theory such as theirs involving resonance such an increased variation in stiffness was, of course, essential.

By contrast, Békésy's direct measurement of volumetric stiffness had been suspect for two reasons:

(i) the excess pressure applied in the scala vestibuli (with the helicotrema blocked) was far too large in relation to any pressure differences occurring normally in the cochlea (it was, indeed, enough to produce a displacement of about 0·01 mm at the point of observation; which required pressure differences from 1 cm of water at the apex to 100 cm at the base);

(ii) the measurement of volume displacement was made on Reissner's membrane rather than on the basilar membrane itself; whereas the volumetric displacements of Reissner's membrane and the basilar membrane need not be the same if the applied pressure difference produces displacement of endolymph in the scala media.

To sum up, the principal data (Békésy 1941) which would tend to make a critical-layer resonance theory (of the type first set out by Peterson & Bogert (1950)) untenable are not only in contradiction to Békésy's own later data but also open to grave objections with regard to the experimental methods used.

Two decades later, the special importance of Peterson and Bogert's contribution was pointed out by Schroeder (1973) and Zweig (1976), who showed how their one-dimensional travelling-wave model with resonance, if only lightly damped, would exhibit features close to those which Rhode (1971) had measured, both as regards amplitude and phase. At the same time, they made the model much easier to use. Briefly, they noticed that, if the WKB approximation were made, and if also the relatively modest variation in fluid cross-sectional area along the length of the cochlea were neglected, then a simple analytic solution of the equation for p could be found, in place of the cumbersome numerical solution of Peterson & Bogert (1950). This analytical solution enabled them to work out simple forms for many interesting quantities. In particular, Schroeder's solution for the cochlea's transient response can

† Later, more detailed analysis of the Békésy data using hairs, by Steele (1976) and others, indicates a stiffness variation by about *four* orders of magnitude.

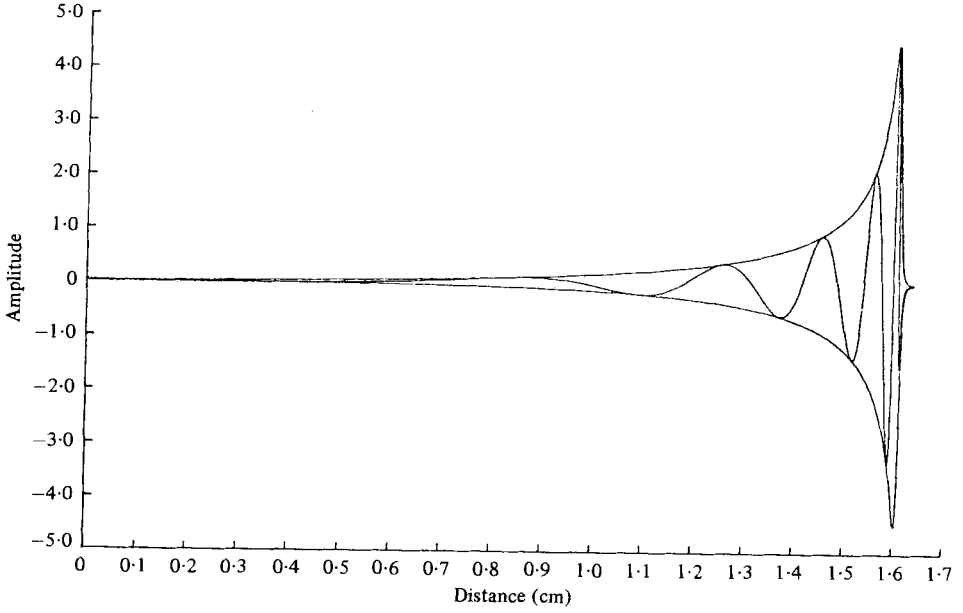

FIGURE 2. Reconstruction by Zweig (1976) of the travelling waves on a squirrel monkey's basilar membrane excited by a pure tone of 70 dB amplitude at 2 kHz. (The displacement curve for the travelling wave is shown at one instant of time; the envelope of the travelling wave is also given.) This reconstruction is computed from the measurements of amplitude and phase by Rhode (1971). The assumption used to interpolate between Rhode's measurements at different points of the membrane is that phase is a function of ω/ω_r (see § 10 for a further discussion of this assumption). For the sake of clarity, the vertical scale is enormously enlarged (the observed maximum amplitude of vibration was around 10^{-5} mm).

be regarded (appendix C) as having, essentially, predicted experimental results like those of Robles *et al.* (1976) already referred to.

Use of the WKB approximation in Schroeder's solution is acceptable, as noted earlier, for frequencies over 1 kHz. Furthermore, it should be usable also at lower frequencies except in a short region near the base where it can be replaced by the Zwislocki solution (with which it matches well).

Zweig (1976) emphasized the effectiveness (in the above sense) of the WKB approximation (see also Zweig *et al.* (1976)) and the utility of the associated solution for explaining the data of Rhode (1971). He also checked that the phase and amplitude measurements of Rhode were consistent with the general properties of causal linear systems. Furthermore, he combined Rhode's experimental data on phase and amplitude at *two* positions on the basilar membrane with an empirical formula allowing interpolation between them to construct remarkable diagrams of the basilar-membrane displacement curve (his figures 6 and 7, the second of which is here reproduced as figure 2). These give a very strong impression of how critical-layer absorption works: as the energy flow slows down ahead of the resonant point there is a piling-up of the energy, after which all the dissipation occurs in a very short final distance (which, however, in energy-flow terms corresponds to a very long final time).

7. Two-dimensional models

A principal motive for giving the above rather full review of the literature on one-dimensional models of cochlear mechanics has been to explain wny a 'good' one-dimensional model, such as that of Schroeder (1973) and Zweig (1976), reflects so accurately the main observed features of basilar-membrane motion in spite of its gross over-simplification of the fluid mechanics. The reason is that a 'good' one-dimensional model can and does exhibit the essential property of critical-layer absorption. A model with this property, and with values chosen for the inertia and stiffness of the cochlear partition which give a realistic distribution of characteristic frequency along the cochlea, has a good chance of representing basilar-membrane motions quite well.

Nevertheless, there is no exaggeration in describing a one-dimensional representation of cochlear fluid mechanics as a gross over-simplification. The physical laws governing fluid motion in an elongated duct, such as the scala vestibuli (or scala tympani), are well known. The associated conditions governing whether or not such motion is effectively one-dimensional when excited by vibrations on just one boundary of the duct (that is, vibrations of the cochlear partition) are also well established (see, for example, Lighthill 1978). For one-dimensional motions the wavenumber k must be less than an upper limit which depends only on the dimensions of the duct cross-section, and is about $0{\cdot}7\ \mathrm{mm}^{-1}$ for a human cochlea (appendix D). Waves with wavenumber exceeding this upper limit involve fluid disturbances (including both motions *and* excess pressures) that are stronger near the vibrating boundary than elsewhere. Then, as the wavenumber k increases still further, the fluid disturbances become essentially limited to a smaller and smaller neighbourhood (of depth k^{-1}) around the vibrating partition.

These well-established properties of waves in fluids have one very clear implication for mathematical models of cochlear mechanics. Such models, if they are to be effective, must exhibit critical-layer absorption (§ 4), which in turn means that the wavenumber k at a fixed point must become large as the characteristic frequency is approached. Evidently, for the human cochlea, once k exceeds $0{\cdot}7\ \mathrm{mm}^{-1}$, the assumption of one-dimensional fluid motion becomes seriously inaccurate.

Note, however, that the WKB approximation is good whenever k exceeds $0{\cdot}2\ \mathrm{mm}^{-1}$ (appendix C). Accordingly, in the only region ($k < 0{\cdot}2\ \mathrm{mm}^{-1}$) where the WKB approximation is unsuitable, we *are* free to use a one-dimensional model (in practice, that of Zwislocki as in appendix C). Conversely, at wavenumbers $k > 0{\cdot}2\ \mathrm{mm}^{-1}$ the WKB approximation becomes accurate, but at wavenumbers $k > 0{\cdot}7\ \mathrm{mm}^{-1}$ it must be combined with a treatment in two or three dimensions.

Until these facts were recognized, notably by Steele (1974, 1976), attempts to produce mathematical models of cochlear mechanics in more than one dimension had been somewhat unenlightening. That was because the difficulties of mathematical analysis could be overcome only if the models were made geometrically very simple. Even then, the still very intricate analysis allowed no clear physical interpretation which could give guidance on how well the conclusions would apply in a cochlea of realistic geometry.

To this day, in fact, the only models avoiding the WKB approximation which go beyond a one-dimensional treatment have been purely two-dimensional models for

ducts of uniform rectangular cross-section. The assumption of two-dimensional motion, of course, ignores the fact that the vibrating basilar membrane occupies only part of the cochlear partition. It supposes the whole width of the cochlear partition to vibrate with uniform amplitude. These are severe limitations. Nevertheless, two-dimensional models based on them, developed by Lesser & Berkley (1972) and perfected by Allen (1977), are able to exhibit many realistic features. These include a transition from a one-dimensional travelling-wave motion near the base, with all the perilymph in a cross-section of a scala moving as one, to a wave of much higher wavenumber with the fluid motion confined to a neighbourhood of the vibrating membrane.

Two-dimensional models were pioneered in the much earlier work of Ranke (1950), whose oversimplified analysis, however, is applicable only *after* that transition has been completed. A modern form of Ranke's treatment (Siebert 1974) is still too complicated to allow of clear physical interpretation, and so has no advantage over the rigorous two-dimensional analysis of Allen (1977); see also de Boer (1979) and Viergever (1980).

Just as the best one-dimensional models (Schroeder 1973; Zweig 1976) reproduce the essential features of basilar-membrane response at moderate stimulus levels, so does the best available two-dimensional model (Allen 1977). Steele & Taber (1979*a*) took an important first step towards understanding physically why this is. They pointed out that in the Allen model all the conditions for applicability of the WKB approximation are amply satisfied, and went on to verify that a quite straightforward analysis of Allen's model using that approximation gives results in good agreement with Allen's.

From the energy-flow standpoint, this WKB approximation states that the energy of the wave travels at the group velocity given by the slope of the frequency–wavenumber plot. The type of plot needed for critical-layer absorption (figure 1*b*) requires the frequency at each position to rise towards the local resonant frequency as the wavenumber becomes large. By a simple extension of the classical formula (2) for that local resonant frequency, we can readily understand why both one-dimensional and two-dimensional models can exhibit this behaviour.

Physics tells us, in fact, that the simple formula (2) relating frequency to stiffness and inertia remains correct even for complicated modes of vibration, provided that (i) the stiffness includes all contributions from forces tending to restore the system to its undisturbed state; and (ii) the inertia includes all contributions from masses which have to be set in motion to allow the system to change its state. Furthermore, in both cases it is contributions to *energy* that are relevant (potential energy for the restoring forces and kinetic energy for the masses) for defining the stiffness and inertia. Whatever *measure* of departure from the undisturbed state is used (such a measure is most commonly called 'generalized co-ordinate' in vibration theory) these definitions are as follows:

$$\text{potential energy} = \tfrac{1}{2}(\text{stiffness})\,(\text{generalized co-ordinate})^2; \tag{3}$$

$$\text{kinetic energy} = \tfrac{1}{2}(\text{inertia})\,(\text{generalized velocity})^2; \tag{4}$$

where the generalized velocity of the system is the rate of change of generalized co-ordinate. For duct flows as in the cochlea, the energies in (3) and (4) should be taken as energies per unit length of duct.

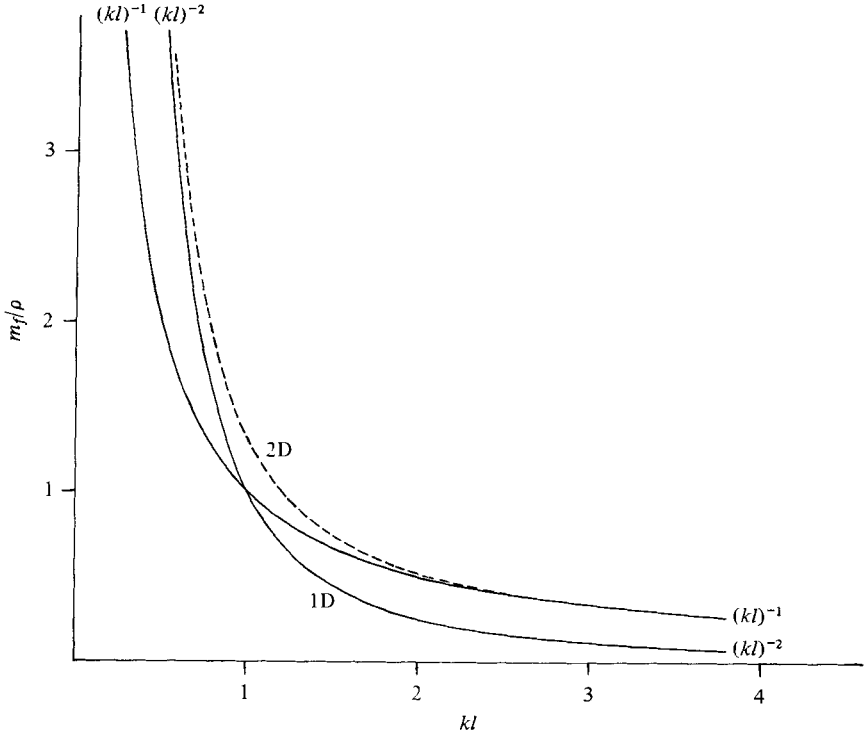

FIGURE 3. Fluid inertia divided by fluid density, plotted against kl for one-dimensional (1D) and two-dimensional (2D) models. Here, k is wavenumber and l is the height of a scala, assumed to be half its breadth. The 1D curve is simply the graph of $(kl)^{-2}$. The 2D curve (broken line, representing a simple function $I(kl)$ defined in appendix D) takes this form for kl less than about 0·5, but for larger values of kl moves over to coincide with the graph of $(kl)^{-1}$. Corresponding curves for 3D models (§9 and appendix E) make a broadly similar transition between the $(kl)^{-2}$ curve for small kl and a form proportional to $(kl)^{-1}$ for large kl. [For a different assumed ratio of scala height l to half-breadth, the curves marked 1D and 2D must simply be scaled up by that ratio.]

The *volumetric* stiffness used in one-dimensional models satisfies (3) if the 'generalized co-ordinate' used to measure departures from the undisturbed state is the volume change in a scala (say, the scala tympani) per unit length of duct. This stores a potential energy equal to the volume change times half the opposing pressure difference (half so as to give the *average* of the opposing pressure difference as the volume change rose from zero to its present value). Then (3) makes the stiffness equal to the volumetric stiffness defined in (1).

It remains satisfactory to use the same generalized co-ordinate in two-dimensional models; and, then, the stiffness defined in (3) continues to be the volumetric stiffness (1). However, the inertia defined in (4) becomes a sum of two terms: the corresponding inertia of the cochlear partition itself (used in (2) to specify the resonant frequency) and the inertia associated with the fluid motions. Thus, we can write the local radian frequency ω as

$$\omega = \left(\frac{\text{volumetric stiffness}}{\text{partition inertia} + \text{fluid inertia}}\right)^{\frac{1}{2}}. \tag{5}$$

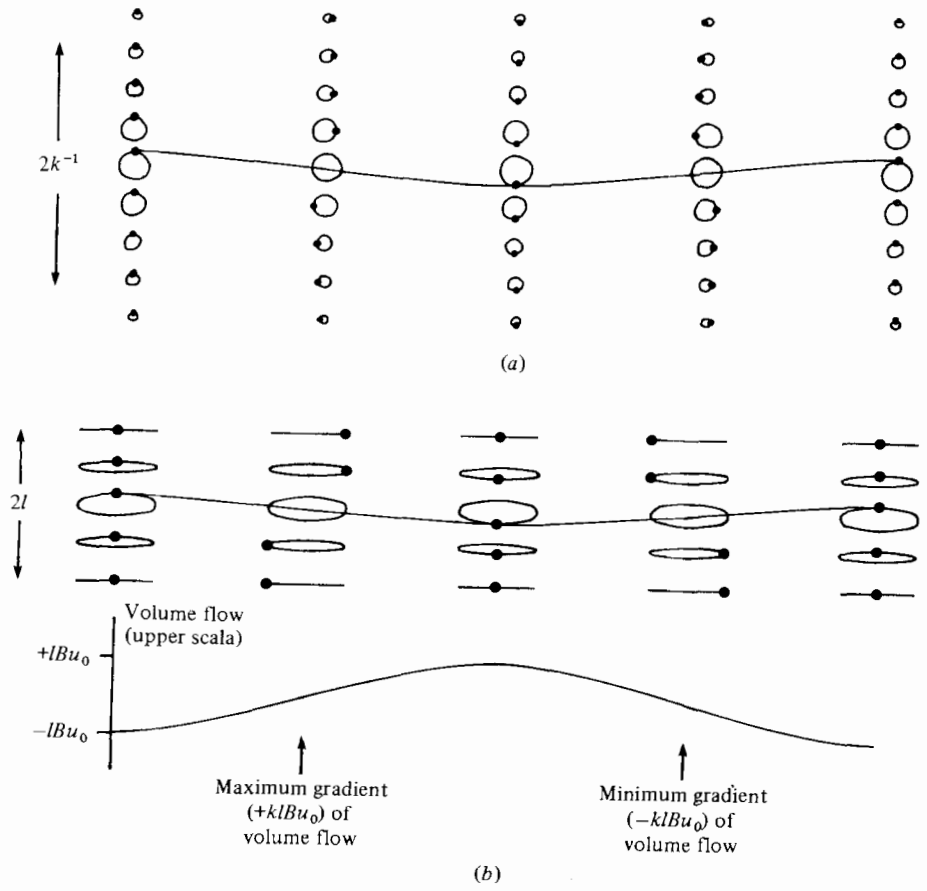

FIGURE 4. (*a*) Motion of particles of fluid predicted by two-dimensional models when a locally sinusoidal wave with relatively *large* values of kl (product of wavenumber and height of a scala) propagates from left to right along the cochlear partition. Each circular particle path is followed clockwise in the lower scala and anticlockwise in the upper scala. The particle's instantaneous position on each path is shown. (*b*) The upper diagram shows the fluid motion predicted by two-dimensional models when a locally sinusoidal wave with relatively *small* values of kl propagates along the cochlear partition (same notation as in (*a*)). The lower diagram plots the volume flow of fluid to the right in the upper scala, of breadth B and height l, with velocity amplitude u_0. The transverse velocity of the membrane must reach its maximum value, klu_0, where the gradient of this volume flow takes its maximum value, $klBu_0$. [In both (*a*) and (*b*), of course, amplitudes of motion are enormously exaggerated for the sake of clarity.]

In two-dimensional models the fluid inertia, relating the fluid kinetic energy per unit length of duct to half the square of the rate of change of scala volume per unit length as in (4), is a certain well-known, and analytically simple, function of wavenumber plotted in figure 3. For values of k exceeding about 2·0 mm^{-1} (a wavenumber derived as 1·5 divided by the height l assumed for the rectangular scala) the graph of fluid inertia, non-dimensionalized as in figure 3, coincides with the graph of $(kl)^{-1}$. This is proportional to the effective depth of penetration, k^{-1}, of the disturbances into the fluid in that high-wavenumber regime.

By contrast, for wavenumbers k less than about 0·7 mm^{-1} (a figure quoted earlier, and here specified as $0{\cdot}5l^{-1}$) the graph of fluid inertia coincides with that calculated

by one-dimensional theory; and, as that theory would also predict, the associated kinetic energy of fluid fills the duct almost uniformly. At first sight this last circumstance might be supposed to lead to a fluid inertia independent of k; but this supposition would be seriously in error, for a reason which must be explained.

For $k > 1{\cdot}5l^{-1}$ the fluid motions (figure 4*a*) are effectively limited to a region within a distance k^{-1} of the vibrating partition. (This is less than the height l of the scala.) Furthermore, individual particles of fluid in that region have *equal* amounts of kinetic energy in their longitudinal motions (along the duct) and their transverse motions (in the plane of the cross-section). Now, the generalized velocity (rate of change of scala volume per unit length) is equal in two-dimensional models to the duct breadth B times the transverse fluid velocity at the vibrating partition. The *total* kinetic energy is twice the kinetic energy in transverse motions only, and this is related to the transverse velocity squared multiplied by the extent k^{-1} of the disturbances. It is not surprising, therefore, that the fluid inertia defined by (4) takes the form of a multiple of k^{-1}.

By contrast, the one-dimensional motions occurring for $k < 0{\cdot}5l^{-1}$ are almost purely longitudinal (figure 4*b*). Nevertheless, at the partition itself, the ratio of transverse to longitudinal velocity amplitudes cannot be zero, but must take the (admittedly, relatively small) value kl. This is because oscillating longitudinal velocities with wavenumber k imply oscillating *gradients in fluid volume flow*, of amplitude kl times the velocity amplitude times the duct breadth. Such gradients in volume flow are in turn possible, of course, only as a result of volume displacements of the partition; in fact, dividing them by the duct breadth gives the amplitude of the transverse velocity at the partition.

Relative to the generalized velocity, then, the velocity amplitude of the main longitudinal disturbances is greater by a factor $(kl)^{-1}$; accordingly, the associated kinetic energy involves this factor *squared*. That explains why the fluid inertia makes a transition (figure 3) from its $(kl)^{-1}$ dependence for large kl to a $(kl)^{-2}$ dependence for small kl.

8. Comparison of different models

The class of mathematical models which can exhibit critical-layer absorption is rather precisely defined by:

(i) figure 1 (*b*) showing the required behaviour of the frequency–wavenumber plot;

(ii) equation (5) relating frequency to stiffness and two kinds of inertia;

(iii) figure 3 showing the dependence of fluid inertia on wavenumber;

(iv) the fact that partition inertia, for a given mode of vibration of the partition, must be independent of wavenumber.

Models with this partition inertia neglected were abandoned (sections 5 and 6) as incapable of defining a resonant frequency (2). We divide the remaining models into

(*a*) those with the volumetric stiffness independent of wavenumber; and

(*b*) the rest.

The wide class (*a*), of models with stiffness independent of wavenumber, is immediately seen by (ii), (iii) and (iv) above to produce a wavenumber plot of the type (i) characteristic of critical-layer absorption for both one-dimensional and two-dimensional models. In fact, as k becomes large, the total inertia in the denominator of (5)

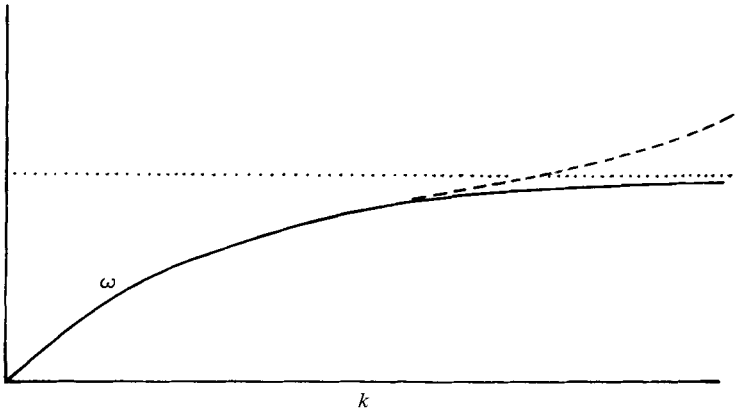

FIGURE 5. Explaining the failure of models which take into account longitudinal stiffness. Plain line: behaviour of the frequency (5) if the volumetric stiffness (1) is independent of k, while the fluid inertia tends to zero with increasing k as in figure 3. Broken line: changed behaviour of the frequency (5) if the volumetric stiffness (1) contains increasing terms (proportional to k^2 and k^4) associated with longitudinal stiffness. The slope U of this line (group velocity at which the wave transmits energy) no longer decreases to zero, so that critical-layer absorption is impossible.

is gradually reduced to the partition inertia, so that the frequency (5) rises to become equal to the resonant frequency (2).

This makes it clear why *both* one-dimensional *and* two-dimensional models meet the central requirement of critical-layer absorption *provided* that the volumetric stiffness (1) is independent of wavenumber. In fact, differences between the predictions of such models involve subtler (albeit significant) features, which depend (see below) on different results of a 'fast' (like $(kl)^{-2}$) or 'slow' (like $(kl)^{-1}$) rise to the resonant frequency.

In the meantime, it has to be noted categorically that models in class (*b*), with stiffness dependent on wavenumber, are incapable of exhibiting critical-layer absorption. This is one of the most important conclusions of the present analysis and therefore demands a full explanation.

The point is that the theory of elasticity clearly defines any dependence of the volumetric stiffness (1) on the wavenumber k as taking the form of an *increase as k becomes large*. The value of (1) when k is small can be described as the transverse stiffness, associated with deformations of the partition which are almost in phase at neighbouring stations so that the elastic potential energy is associated only with transverse, and not with longitudinal, bending. To that transverse stiffness may be added (as k increases) terms in k^2 and k^4 associated both with any longitudinal tension in the membrane and with any longitudinal bending stiffness. No doubt the presence of longitudinal stiffness terms, involving additions to the potential energy as the longitudinal waviness of the basilar membrane increases, is to be expected. Nevertheless, the mathematical models that represent cochlear vibrations most successfully are those that allow no such increase of stiffness with wavenumber, and the present analysis shows clearly why that is, as follows.

In fact, the frequency–wavenumber plot can take the form shown in figure 1 (*b*) as necessary for critical-layer absorption *provided* that the stiffness does not increase as

k becomes large. Only then will the frequency (5) tend to a well-defined resonant frequency as the fluid inertia tends to zero for large k. By contrast, if simultaneously the stiffness is increasing, the plot will curve upwards (figure 5) and fail to show many essential features such as high-frequency cutoff and continued slowing down of energy flow.

The original paper of Huxley (1969), that suggested a combination of travelling-wave and resonance theories, recognized the above difficulty (that natural assumptions about longitudinal stiffness can destroy the possibility of resonance) but suggested that the elastic stress system of the basilar membrane may be more complicated than that in a classical 'elastic plate'.† Certainly, the natural tendency of stiffness to increase with k would be greatly reduced if the membrane as held by the bony shelf and the spiral ligament were subject to a *longitudinal thrust* (negative tension). Such a longitudinal thrust along the length of the cochlea would produce a reduction in potential energy with increasing k that could largely cancel the increase due to longitudinal bending stiffness (at least for practically interesting values of k, at which the main critical-layer absorption process is occurring). Yet another possible explanation of why transverse stiffness may greatly exceed longitudinal stiffness in significance is to be found in the suggestions of Steele (1974, 1976) on the important contribution to transverse stiffness made by the properties of the 'hinge' where the basilar membrane is attached to the bony shelf via the arch of Corti.

To sum up, an effective mathematical model of cochlear mechanics requires that both the stiffness and the inertia of the cochlear partition are effectively independent of wavenumber so that they define a resonant frequency (2). At the same time, its other requirement, of a fluid inertia tending to zero as wavenumber increases, is satisfied both by a one-dimensional, and by a two-dimensional model (figure 3). On the other hand, the assumptions underlying a one-dimensional model are certainly violated once the wavenumber k exceeds quite a modest value around $0{\cdot}7\ \mathrm{mm}^{-1}$.

Actually, a mathematical model needs to satisfy two requirements if it is to lead to valuable understanding of cochlear mechanics. First, the model must fulfil the conditions for critical-layer absorption so that its conclusions will not contradict the results of observations of basilar-membrane vibration at moderate stimulus levels. Secondly, the model must avoid contradicting other well-established facts. It is on that basis that one-dimensional models must be discarded. Furthermore, this will prove significant for defining the detailed nature of the critical-layer absorption in the cochlea because of differences in the implications of a fluid inertia tending to zero 'fast' (like $(kl)^{-2}$ as in one-dimensional theory) or 'slow' (like $(kl)^{-1}$).

9. Three-dimensional models

Continuing to apply, as it were, such a 'second filter' to the available mathematical models, it is perhaps logical to reject also two-dimensional models. That is because they unrealistically assume fluid velocities which vary only with distance from the

† The experimental evidence accumulated by Békésy (1960) suggesting such an 'elastic plate' model was, of course, obtained in cadavers; but comparisons (Rhode 1973; Kohllöffel 1973) of basilar-membrane stiffness properties in the same animal before and after death showed significant changes. Much more recently, the work of Voldřich (1978) has confirmed experimentally that the basilar membrane *in vivo* has negligible longitudinal stiffness; and, also, has shown that longitudinal stiffness quickly becomes significant after death.

cochlear partition. Actually, variation across the width of that partition is likely to be very pronounced. For example, fluid close to the basilar membrane is likely to move much more than fluid near the bony shelf; while, over the membrane itself, a maximum disturbance towards its *centre* is to be expected.

Fortunately, the work of Steele (1974, 1976) shows clearly that a far more realistic three-dimensional model is relatively easy to construct if the WKB approximation is used (see also Steele & Taber 1979*b*). In that context, the accurate work of Allen (1977) on a two-dimensional model gains importance from its use by Steele & Taber (1979*a*) to demonstrate how *well* the WKB approximation reproduces accurate data for a problem where those are known.

In the present paper's language, Steele effectively calculated the fluid inertia for a three-dimensional model (see appendix E). On the whole, a model using this calculated value for fluid inertia, together with distributions of partition inertia and stiffness along the cochlea which are independent of wavenumber, seems to combine best the essential requirement for critical-layer absorption with a demand for maximum realism within that limitation.

As would be expected, the Steele calculation of fluid inertia shows some variation, not only with kl as in figure 3, but also with another parameter which varies along the cochlea. This is the *proportion* of the breadth of the cochlea taken up by the basilar membrane. Nevertheless, though the curves for different values of that parameter are different (appendix E), they do all share the property highlighted in figure 3; that is, they make a transition from behaviour like $(kl)^{-2}$ for small kl to behaviour in proportion to $(kl)^{-1}$ for large kl (and, essentially, for the same physical reasons).

The preferred three-dimensional type of model, then, shares with two-dimensional models this property of a relatively *slower* decay of the fluid inertia to zero (as k becomes large) than one-dimensional models would suggest. Consequently, although all three types of model satisfy the main requirement (prediction of critical-layer absorption) there are various local differences of some significance between one-dimensional and multi-dimensional models in the type of behaviour predicted near the critical layer.

First, a multi-dimensional model allows a more rapid growth of wavenumber k as a wave of given frequency ω approaches the point where ω coincides with the resonant frequency ω_r. In fact (appendix E), k varies as $(\omega_r - \omega)^{-1}$.

Already this partly explains the accuracy of the WKB approximation because it allows the growth of wavenumber to *keep pace* (as that approximation demands) *with the relative longitudinal rate of change of wavenumber*. By contrast, the one-dimensional models have k varying as $(\omega_r - \omega)^{-\frac{1}{2}}$ only, when as Zweig *et al.* (1976) point out the WKB approximation could break down in the case of extremely small damping.

Next, the passage of wave energy of frequency ω to a position where the resonant frequency is ω_r takes a time increasing like $(\omega_r - \omega)^{-1}$ for the multi-dimensional models, but (just as with k) only like $(\omega_r - \omega)^{-\frac{1}{2}}$ for one-dimensional models. In this respect, also, the multi-dimensional models are rather better adapted to work satisfactorily (giving massive energy absorption in that quite long time) with only light damping.

Lastly, the build-up of basilar-membrane vibration amplitude, before damping becomes significant, is predicted as proportional to $(\omega_r - \omega)^{-1}$ on the multi-dimensional theories. This, too, seems a satisfactory representation of the observed data (appendix

E), although the difference from one-dimensional models (which predict $(\omega_r - \omega)^{-\frac{3}{4}}$) is less marked on this point.

Within the class of multi-dimensional models, the fully three-dimensional models possess one special feature, which has definite interest and is demonstrated at the end of appendix E. They tend to show a certain anticipatory slowing down of energy propagation to occur as a forerunner of its final bringing to a halt at the point of resonance.

10. Conclusions for frequencies a little below the characteristic frequency

The suggestion that realistic three-dimensional models of a type allowing critical-layer absorption may be specially good accounts of the amplitude and phase data near resonance is encouraging. With that background, it may be desirable to indicate in more detail the predicted behaviour on the immediate low-frequency side of the characteristic frequency. That is the region where loudness discrimination between two rather loud pure tones of the same frequency may possibly originate (Laming 1979); this possibility assumes that, for loud pure tones, neurones associated with the site where their frequency is the characteristic frequency may be saturated. That would put the burden of discrimination on neurones associated with sites where the tones' frequency is close to, but on the low-frequency side of, the characteristic frequency.

In this region, the analysis of appendix E suggests that a number of significant properties of the basilar-membrane vibration depend on the *ratio* ω/ω_r of the vibration's frequency ω to the local resonant frequency ω_r. It is interesting that Zweig (1976) proposed such a dependence on ω/ω_r for various quantities (especially, the phase) as a reasonable basis for interpolation between the patchily available experimental data. This is the basis on which figure 2 was built up by Zweig from the experimental data of Rhode (1971). That assumption is now seen to be valid for a three-dimensional model as well as for models of the one-dimensional type described in another part of Zweig's paper.

Figure 6 shows how key variables are predicted to behave at a point as a function of ω/ω_r on the immediate low-frequency side of the resonant frequency ω_r. The graph marked (*a*), representing

$$(\omega/\omega_r)^2/[1-(\omega/\omega_r)^2], \tag{6}$$

indicates the predicted behaviour of *both* the number of wave periods taken for energy of frequency ω to reach the point *and* the wavenumber k associated with that energy (each, of course, on an appropriate scale). Similarly, the graph marked (*b*), representing

$$\ln[1-(\omega/\omega_r)^2], \tag{7}$$

describes the behaviour of the phase on an appropriate scale.

Finally, the graph marked (*c*), representing

$$\frac{(\omega/\omega_r)^{\frac{1}{2}}}{1-(\omega/\omega_r)^2} \tag{8}$$

on a logarithmic scale, indicates the behaviour of the 'amplitude intensification factor' near resonance. Such an amplitude intensification factor describes intensification of amplitude *relative to* what a simple one-dimensional model without resonance

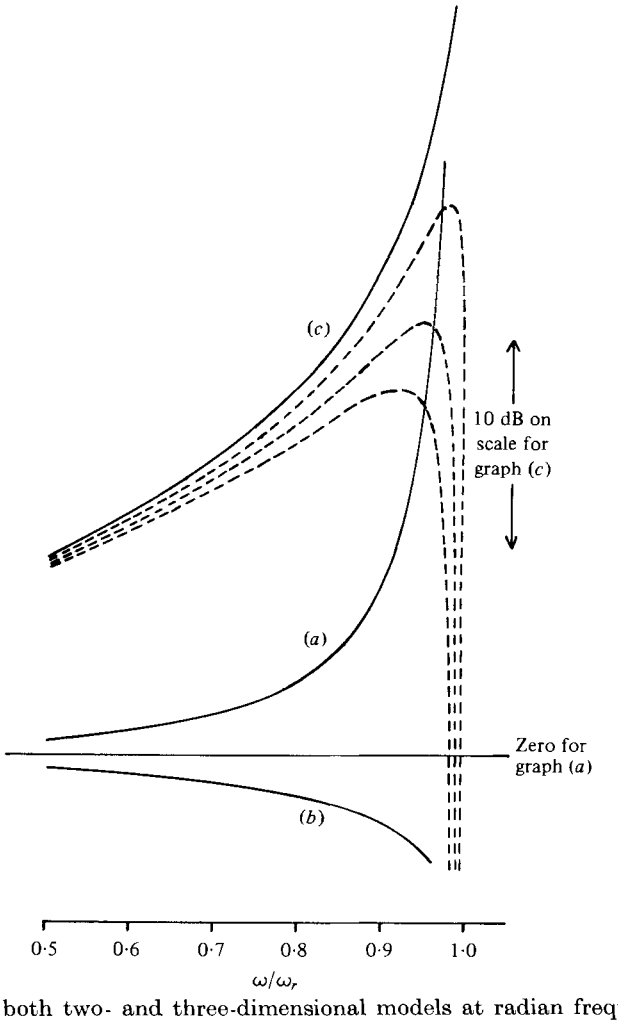

FIGURE 6. Results for both two- and three-dimensional models at radian frequencies a little below the resonant frequency ω_r. (*a*) Graph of expression (6), representing (each on an appropriate scale) *both* the number of wave periods taken for energy of frequency ω to reach the point where the resonant frequency is ω_r *and* the wavenumber k associated with that energy. (*b*) Graph of expression (7), representing (on an appropriate scale) the corresponding variation of phase. (*c*) Amplitude intensification (on the decibel scale shown) relative to what a simple one-dimensional model without resonance (or damping) would predict. Broken lines: corresponding curves with three different damping constants (in the ratio 1:2:3). [Note that the zero line shown is relevant only to graph (*a*).]

(the Zwislocki model of § 5 or appendix C, but with damping omitted) would produce.† Broken lines indicate modifications of this graph which result if wave energy is taken to be dissipated at various rates with respect to *time* (as given by graph (*a*)). Three different proportional rates of dissipation are used.

To give a final summing up, considerations of energy flow in the cochlea force the analyst to adopt a mathematical model with critical-layer absorption. One-dimen-

† At frequencies above about 1 kHz, this is the familiar gain of 6 dB/octave.

sional models are seriously deficient near the characteristic frequency. Two-dimensional models make use of unrealistic assumptions but are valuable for two reasons. First, they allow an excellent check that the WKB approximation has good accuracy. Secondly, a much more realistic three-dimensional model analysed according to WKB approximation gives, in the important region of frequencies just below the characteristic frequency, results (summarized in figure 6) which coincide with those of a two-dimensional model. Anomalous features in the loudness discrimination of pure tones, often described as the 'near-miss to Weber's law', have recently been analysed in the light of the above conclusions by Laming (1979).

I am most grateful to Dr E. de Boer, Dr R. MacKay, Dr C. R. Steele and Dr G. Zweig for their great kindness in giving me extremely valuable suggestions and comments on my work. In addition, my warmest thanks are due to Dr D. R. J. Laming for the exceptionally extensive help and advice which he so patiently gave me at all stages of my investigations in this field.

Appendix A. Effects of fluid compressibility

Most mathematical models of cochlear mechanics have neglected the compressibility of the cochlear fluids. The work of Peterson & Bogert (1950), however, was a notable exception, suggesting that compressibility effects could significantly affect cochlear fluid motions at the highest audible, or lowest ultrasonic, frequencies. Their model, of course, was strictly one-dimensional. This appendix extends their analysis to multi-dimensional models. It indicates that the cochlear response is in two parts, only one of which is influenced by compressibility. Furthermore, this part remains one-dimensional in character even when the other part (uninfluenced by compressibility) has a strongly multi-dimensional distribution.

We can begin to understand this most readily by recalling how sound would be propagated in a cochlea that was devoid of any cochlear partition and was filled entirely with perilymph. Then the thick temporal bone could be viewed as effectively a rigid boundary since its distensibility is much less than the compressibility of the perilymph. Wave motions travelling along such a rigid waveguide are known (see for example Lighthill 1978, p. 420) to be purely longitudinal (that is one-dimensional) at radian frequencies ω below a certain limiting value ω_m. This is the low-frequency cutoff for transverse-mode propagation. The corresponding frequency in hertz, $f_m = \omega_m/2\pi$, takes the values

$$f_m = 0{\cdot}29c_0/l \quad \text{or} \quad 0{\cdot}25c_0/l \tag{A 1}$$

for a circular cross-section of diameter $2l$ or a rectangular cross-section of length $2l$, respectively; here, $c_0 = 1400$ m s^{-1} is the speed of sound in perilymph. Evidently, with cross-sectional diameters less than 2 mm as in the cochlea the value of f_m is well over 300 kHz.

At all interesting frequencies, then, the only waves that could propagate along a cochlea devoid of any partition and filled with perilymph alone would be *one-dimensional* sound waves. In these, the pressure is uniform over each cross-section of the cochlea, and only varies longitudinally (that is, from base to apex) and with time. We shall find that the introduction of a cochlear partition does not suppress

these waves. Instead, it allows them to be combined with a second group of waves whose propagation is uninfluenced by compressibility because for them the mean pressure over each cross-section is zero.

Peterson & Bogert established this fact only for strictly one-dimensional motions; that is, for motions where the pressure takes a uniform value p_1 throughout that part of a cross-section which lies on one side of the cochlear partition, and a different uniform value p_2 throughout the part which lies on the other side. They found that the deduction is made most simply in the case when both those parts are taken to be of the same cross-sectional area $A(x)$; which, however, may be allowed to decrease gradually as the distance x from the base increases. We reproduce their deduction with this simplification retained because differences between cross-sectional areas on either side of the cochlear partition appear in general to be rather small.

The volume flow of fluid from base to apex is taken to be J_1 on one side of the cochlear partition and J_2 on the other. The linearized equations of fluid momentum on the two sides become

$$\rho_0 \partial J_1/\partial t = -A\,\partial p_1/\partial x, \quad \rho_0 \partial J_2/\partial t = -A\,\partial p_2/\partial x, \tag{A 2}$$

where ρ_0 is the undisturbed density of the fluid. Here, $\partial J_1/\partial t$, for example, is equal to the cross-sectional area A times the local fluid acceleration, and the first equation relates this appropriately to pressure gradient.

Any spatial downward gradient in volume flow such as $(-\partial J_1/\partial x)$ must result from a local rate of change of fluid volume associated with either the fluid's compressibility K or the distensibility of the tube. This distensibility, D, is defined for a *single isolated tube* as the proportional increase in cross-section area per unit increase in pressure. This gives

$$-\partial J_1/\partial x = A(D\,\partial p_1/\partial t + K\,\partial p_1/\partial t), \tag{A 3}$$

as a sum of the rate of increase of *tube volume* per unit length (that is, of cross-sectional area) and a correction for the increasing quantity of fluid which, when the pressure is increasing, can be fitted into unit length without any such change in tube volume. The combination of equation (A 3) with the first of equations (A 2) gives the well-known result (Lighthill 1978, p. 93) that waves propagate at a speed

$$[\rho_0(K+D)]^{-\frac{1}{2}}, \tag{A 4}$$

depending on the *sum* of the fluid's compressibility and the tube's distensibility.

Equation (A 3), however, is significantly modified in the case of two adjacent tubes that undergo equal and opposite cross-section variations proportional to the *difference* of pressure across the partition between them. If in this case we define D as the proportional increase in cross-sectional area of either tube per unit *excess* of the pressure in that tube over the pressure in the other, then (A 3) is evidently replaced by the following two equations:

$$-\partial J_1/\partial x = A[D\,\partial(p_1-p_2)/\partial t + K\,\partial p_1/\partial t], \quad -\partial J_2/\partial x = A[D\,\partial(p_2-p_1)/\partial t + K\,\partial p_2/\partial t]. \tag{A 5}$$

If now we write

$$p_1 = P+p, \quad p_2 = P-p, \quad J_1 = J+j, \quad J_2 = J-j \tag{A 6}$$

so that P and J are the cross-sectional mean pressure and volume flow while p and j are the departures from the means, then equations (A 2) and (A 5) give

$$\rho_0 \partial J/\partial t = -A\,\partial P/\partial x, \quad -\partial J/\partial x = AK\,\partial P/\partial t \tag{A 7}$$

for the means and

$$\rho_0 \partial j/\partial t = -A\,\partial p/\partial x, \quad -\partial j/\partial x = A(K+2D)\,\partial p/\partial t \tag{A 8}$$

for the departures from the means. In other words, P and J satisfy the equations for waves travelling at the classical sound speed

$$c_0 = (\rho_0 K)^{-\frac{1}{2}}. \tag{A 9}$$

By contrast, p and j satisfy equations which describe waves travelling at the speed

$$c = [\rho_0(K+2D)]^{-\frac{1}{2}}. \tag{A 10}$$

These two speeds replace the single speed (A 4) found in the case of a single duct.

The slower wave speed (A 10) is enormously lower in the case of the cochlea. In fact, D exceeds K (even near the base) by such a large factor that to all intents and purposes the speed c of the slow waves is uninfluenced by compressibility and can be written

$$c = (2\rho_0 D)^{-\frac{1}{2}}. \tag{A 11}$$

The propagation of these slow waves is treated in detail in later appendices. Here, we note simply that their speed (A 11) decreases continuously from base to apex. Accordingly, the frequency below which one-dimensional theory gives a good approximation also decreases from base to apex.

Actually, for these slow waves we cannot speak of a precise cutoff frequency as with (A 1) for sound waves, below which propagation is exactly one-dimensional. Nevertheless (appendix D), there does exist a frequency proportional to c/l (with (A 11) now specifying c) below which departures from one-dimensional propagation are less in magnitude than (say) 3 %. This is important because stimulation of the cochlea at frequencies significantly exceeding 100 Hz excites waves which, as they pass from base to apex, ultimately reach a point where this requirement for good accuracy of a one-dimensional analysis ceases to be satisfied.

For these frequencies, then, the assumptions of the above one-dimensional theory are invalid beyond a certain point in the cochlea. Fortunately, however, we can make a fully three-dimensional analysis which leads to the same conclusions for the propagation of the cross-sectional mean pressure P; at the same time, for the departures p of the fluid pressure from this cross-sectional mean, it implies a more complicated (and fully three-dimensional) propagation behaviour which, however, is yet again uninfluenced by fluid compressibility.

The simplest route to this conclusion is to write the fluid pressure as $P+p$, where (i) both P and p may vary over a cross-section, although we shall in fact find that P does not; while (ii) P is an 'even', and p an 'odd' function; that is, P takes equal values with the same sign, and p equal values with opposite signs, at points which are mirror images of each other in the cochlear partition. (This definition makes P the *mean* of the pressures at the two image points.)

Both P and p must satisfy the linearized equation governing small motions of a compressible fluid; this is the acoustic wave equation

$$\partial^2 P/\partial t^2 = c_0^2 \nabla^2 P, \tag{A 12}$$

where c_0 is the sound speed (A 9). Both satisfy, also, the condition of zero normal derivative at the rigid temporal-bone wall of the cochlea. However, P itself has been defined so that it cannot have any discontinuity at the cochlear partition, since its value on either side of it is evidently the same. This, with (A 12), means that P is the solution of the physical problem mentioned at the beginning of this appendix: acoustics in a cochlea without any partition. We know already that at all interesting frequencies (certainly, for those less than 300 kHz) the solution P of that problem is necessarily uniform across a cochlear cross-section. This makes P simply the average pressure over a cross-section (since the other part p of the pressure is an odd function and so has zero average). It, and the corresponding volume flow J, are governed by equations (A 7). These, with c_0 defined in (1.9), give

$$A\,\partial^2 P/\partial t^2 = c_0^2(\partial/\partial x)\,(A\,\partial P/\partial x), \tag{A 13}$$

the well-known area integral of the acoustic wave equation (A 12).

The odd part p of the pressure satisfies, as we have seen, the same equation (A 12) as P but there are two important differences in its properties. Above all, it is discontinuous across the cochlear partition (the discontinuity in p accounting, in fact, for the whole of the pressure discontinuity across the partition). We shall find that this leads to wave speeds c that are extremely small compared with c_0 whether a one-dimensional analysis as above, or a two- or three-dimensional analysis, is used.

Accordingly, the left-hand side of $\partial^2 p/\partial t^2$ of the wave equation (A 12) for p is completely negligible compared with a typical term on the right-hand side such as $c_0^2\,\partial^2 p/\partial x^2$. (In fact, their ratio is as the *square* of this small ratio of wave speeds.) The equation for p reduces, then, to the simpler Laplace equation

$$\nabla^2 p = 0 \tag{A 14}$$

describing fluid motions uninfluenced by compressibility.

Both for one-dimensional and multi-dimensional models, then, we have inferred that the departure p from the cross-sectional mean pressure is uninfluenced by compressibility. In other words, it satisfies the equations (neglecting compressibility) which have been widely used in the literature to describe the whole pressure field in the cochlea. For further analysis of those equations, see later appendices (B and C for one-dimensional models, and D and E for multi-dimensional models).

However, p is *not* the whole pressure field, which in fact includes also the part P satisfying the equation (A 13) of one-dimensional sound waves. This correction is particularly significant near the base, where p and P must indeed be almost equal. This follows from the fact that, at the base, only the motions in the scala vestibuli are forced, by the action of the stapes footplate against the oval window, whereas motions in the scala tympani are subject to no significant forcing. Indeed, the motions of the round window are resisted by a medium of such low density (the air of the middle ear) that the resulting pressure fluctuations $p_2 = P - p$ are negligible compared with those in the perilymph of the cochlea.

Admittedly, p is known to increase steeply with distance from the base (at any rate as far as the position of resonance) while (as we shall see) P normally changes much more gradually. Nevertheless, at the base itself, where the one-dimensional expressions (A 6) are applicable, p and P must be closely equal so that p_2, the pressure fluctuation in the scala tympani, can remain negligibly small.

By contrast, the relationships between volume flows, which we continue to write $J+j$ and $J-j$ as in (A 6), are quite different. This fact, important in the context of *energy flow*, is just one more consequence of the greatly different speeds of propagation of the two signals p and P. Because wave impedance (ratio of pressure to volume flow) is proportional not only to the density (a fact just used in considering the round window) but also to the wave speed, the ratio P/J enormously exceeds the ratio p/j. Accordingly, J is negligibly small even near the base, where P and p are closely equal. This means that to close approximation $J_1 = +j$ and $J_2 = -j$ are equal and opposite. In particular, the volume flows generated by motions of the oval and round windows are equal and opposite, exactly as if the fluid in the cochlea were incompressible, even though the pressure distribution p calculated on incompressible-flow theory falls short of the true pressure distribution by the quite significant difference P.

Energy flow in a tube is the mean product of pressure and volume flow. Thus, in the scala vestibuli where the pressure is $P+p$ and the volume flow $+j$, the energy flow is

$$\overline{Pj}+\overline{pj}; \tag{A 15}$$

whereas, in the scala tympani, where the pressure is $P-p$ and the volume flow $-j$, the energy flow is

$$-\overline{Pj}+\overline{pj}. \tag{A 16}$$

Both expressions include the same term

$$+\overline{pj}, \tag{A 17}$$

signifying energy flow towards the apex in the slow wave, which is necessarily positive according to the strongly supported interpretations of that wave as a travelling wave.

Additionally, expressions (A 15) and (A 16) include first terms

$$+\overline{Pj} \quad \text{and} \quad -\overline{Pj} \tag{A 18}$$

(identical except for sign) associated with interaction between the pressure in the fast wave and the volume flow in the slow wave. These terms resolve an undoubted paradox in the travelling-wave interpretations; namely, that the slow-wave energy flow (A 17) is as great in the scala tympani, where the motions are unforced, as in the scala vestibuli, where forcing by the stapes footplate acts as a source of energy flow. Indeed, at the base, where $p = P$, the equal and opposite terms (A 16) imply that the net energy flow in the scala tympani is zero, whereas the scala vestibuli transmits an energy flow twice as great as it would carry in a pure slow wave. Locally, we might say that it takes charge of the other scala's share as well; although, away from the base, where p increases and P decreases, the distribution of energy flow between them becomes much more even.

Figure 7 illustrates the two components (A 18) (broken lines) and (A 17) (plain lines) of energy flow. The travelling-wave energy flow (A 17), equal in both scalae, is directed away from the base in *both*, even though the only energy input is into the

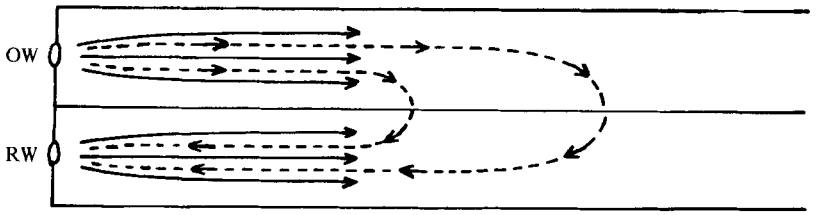

FIGURE 7. Energy flow in two adjacent tubes separated by a flexible partition, with forcing at OW (representing oval window) and negligible impedance to the motion of RW (representing round window). Broken lines: fast-wave energy flow from OW to RW. Plain lines: slow-wave energy flow, equal in amount, travelling *away* from OW and RW in both tubes.

scala vestibuli. This is possible because the fast-wave energy flow (A 18), equal and *opposite* in both scalae, carries energy down the scala vestibuli, across the cochlear partition, and back up the scala tympani to the round window. The cycle of energy flow, totalling what is needed to feed the travelling wave in the scala tympani, is completed between the base and the first 'node' of the slow wave (point where $j = 0$).

Similar considerations of interaction between the fast and slow wave can be used to explain another apparent paradox. Stimulation of a cat's cochlea by an acoustic signal applied at the *apex* was found (Wever & Lawrence 1954, p. 275) to generate distributions of cochlear potentials very similar to those generated with normal stimulation at the base. On the assumption that normal stimulation generates a travelling wave directed from base *to* apex, how could such a wave be produced by stimulation at the apex?

The answer is that the apical stimulation generates an acoustic fast wave which travels quickly to the base, where it encounters a very low impedance at the round window; and, at the oval window, the vastly greater impedance provided by the inertia of the stapes. To a close approximation, *pressure fluctuations* are kept very small at the round window, while *fluid motions* are kept very small at the oval window. The reflected-wave system generated by these boundary conditions consists of (i) a fast wave with equal and *opposite* pressure fluctuations; this satisfies the round-window condition, but produces a doubling of those volume-flow fluctuations at the base which violate the oval-window condition; (ii) a slow wave with volume-flow fluctuations which cancel those at the oval window.

Note that the slow wave has equal and opposite volume flows in the two scalae, so that at the round window the volume flow is *redoubled*. However, motions there are negligibly impeded. Note also that the pressure cancellation at the round window produced by (i) above is not significantly altered by (ii) because, as we have seen, the pressures corresponding to given volume-flow fluctuations are far smaller in the slow wave than in the fast wave.

To sum up, a given acoustic stimulation at the apex leads (by *reflection at the base* of the fast wave it produces) to generation of a slow wave of comparable volume flow, travelling from base to apex. Because basilar-membrane stiffness decreases apically, the pressure fluctuations in this wave increase substantially as it progresses (though not beyond the point of resonance). By contrast, any comparable slow wave generated (along with the fast wave) at the apex suffers the opposite effect: the corresponding pressure fluctuations decrease substantially as it progresses. It is not surprising, then,

that the dominant observed effect is the same base-to-apex travelling wave as is found with normal stimulation.

It may be useful to note typical solutions of the quite simple equations (A 13) and (A 7) for the fast wave subject to pure-tone stimulation at the oval window. The solutions take the form of a *standing wave*

$$P = f(x)\exp(i\omega t), \tag{A 19}$$

where the pressures throughout the cochlea are all in phase. Here, the function $f(x)$ is determined as a solution of the equation

$$(Af')' + \omega^2 c_0^{-2} Af = 0 \quad \text{with} \quad Af' \to 0 \quad \text{at the apex} \quad x = L \tag{A 20}$$

(where x is measured from the base at $x = 0$ in a cochlea of length L). Here, the condition at the apex results from the fact that the overall volume flow J must vanish there. It is this which causes any fast travelling wave to be reflected at the apex as an equal wave travelling in the opposite direction, so that the combination of the two takes the form of a standing wave (A 19) with the same phase at all positions.

For example, if the cross-sectional area A were uniform along the cochlea, the solution

$$f(x) = f(0)\{\cos[\omega c_0^{-1}(L-x)]\}/\{\cos(\omega c_0^{-1}L)\} \tag{A 21}$$

would be appropriate. This exhibits *quarter-wavelength resonance* in the sense that when $\omega c_0^{-1}L$ is near $\frac{1}{2}\pi$ the fast-wave pressure amplitude $f(x)$ at most points in the cochlea becomes large in relation to the pressure amplitude at the base, $f(0)$; which, in turn, is the same for the fast and slow waves (being determined by the slow-wave input impedance). For a cochlea of length 35 mm, this quarter-wavelength resonance is realized at a frequency of 10 kHz.

In a real cochlea, the cross-sectional area A becomes smaller towards the apex, decreasing with x at a roughly constant rate. If we take it proportional to $(L-x)$, so that it decreases linearly to zero at $x = L$, then equation (A 20) gives

$$f(x) = f(0)\{J_0[\omega c_0^{-1}(L-x)]\}/\{J_0(\omega c_0^{-1}L)\}, \tag{A 22}$$

with resonance for $\omega c_0^{-1}L = 2{\cdot}40$ (first zero of the Bessel function J_0); a resonance realized at a frequency of 15 kHz. However, this is probably an overestimate of the resonant frequency. The true variation of A in a typical cochlea shows a linear decrease from its value at the base to only a little under *half* as much immediately before the apex. Peterson & Bogert give a solution with such a distribution of A, and this exhibits resonance at a frequency of 12 kHz; which, therefore, is likely to be the region of frequency for which fast-wave amplitudes may be largest.

At lower frequencies, the fast-wave pressure amplitude $f(x)$ shows a relatively moderate increase from base to apex. The slow travelling wave, starting at the same amplitude, grows much more steeply in amplitude all the way to the point of resonance. There, however, it falls to zero, leaving behind only the fast wave. Effects of the fast wave may, therefore, be found mainly in the region beyond the point of resonance. In that case, at a *fixed* point, they would be found mainly at frequencies above the characteristic frequency.

This is the region where Rhode (1971) observed by his Mössbauer technique basilar-membrane motions quite different from those found below the characteristic frequency. First of all, their amplitudes were orders of magnitude lower. Secondly, and more

surprisingly, the velocities of the Mössbauer source that had been placed upon the basilar membrane were either exactly *in phase* or (rather more commonly) exactly *in antiphase* with the velocities of a separate Mössbauer source placed on the malleus. It is hard to explain this finding in terms of a 'slow' travelling wave, which must suffer a large phase lag, of magnitude sensitively dependent on frequency, between the oval window and the position of measurement.

The analysis of this paper suggests, however, that at frequencies above the characteristic frequency the signal may be dominated by the 'fast' standing wave, which is all at the same phase. Admittedly, the precise response of the cochlear partition to a signal similar to the fast wave is not known. The essential feature of the fast wave is that the pressure on both sides of the cochlear partition is the same; that is, there is no pressure difference to excite the normal *bending* response. It is, however, quite possible that the cochlear partition may move in some different way in response to such a standing-wave pressure fluctuation (equal in both scalae), of uniform phase and apically increasing amplitude. Here, it is important to notice that, if the response is *resistive* (being dominated, for example, by viscous resistance to fluid motions within the narrow tunnel of Corti, forced by the gradient of pressure), then its phase would be consistent with Rhode's observations.

Thus, malleus velocities must generate stapes velocities in phase. These, in turn, produce slow-wave pressures p in phase with the velocity of the stapes (and determined by the slow-wave impedance at the base). But the fast-wave pressure P is constrained to be equal to p at the base. These fast-wave pressures (A 19) have increasing amplitude and uniform phase throughout the cochlea; if the basilar membrane responds resistively to the resulting gradient of pressure (as it would do, for example, if the pressure gradient generated a viscously resisted fluid flow in the tunnel of Corti) then the resulting velocity of the Mössbauer source would be either in phase or in antiphase with the velocity of the stapes, and so also with that of the malleus.† Such a preliminary tentative interpretation may, perhaps, be worth following up.

We conclude this appendix with some brief comments on the response of a cochlea with the scala tympani drained of fluid. Experiments with physical models of the cochlea suggest that this response should be somewhat closely comparable with that found in a normal cochlea. Analysis along the lines of this appendix yields the same conclusion.

We have, indeed, already seen that the main difference in the wave motions to be expected when the scala tympani is drained lies in the absence of any fast wave. On a one-dimensional analysis, we have just one wave speed (A 4) instead of the two wave speeds (A 9) and (A 10). Since D is always much greater than K, we can say that whereas the fast wave speed (A 9) disappears the slow wave speed (A 11) is increased by a factor of $\sqrt{2}$. Physically, this is because the inertia of the system has been halved. The same change in slow-wave speed would be found with fluid present in both scalae if the stiffness of the basilar membrane were *doubled*.

A multi-dimensional analysis leads to the same conclusion. Propagation of the

† By contrast, neither an elastic response nor an inertial response could be regarded as a possible explanation because each would produce motions in quadrature. Only a resistive response would have the right phase. Furthermore, a resistive response in the tunnel of Corti, if present, would have an important damping function, controlling the amplitude of fast-wave motions at the resonant frequency.

slow wave along the real cochlea is specified by Laplace's equation (A 14) together with a condition describing how the displacement of the cochlear partition responds to the pressure discontinuity of $2p$ across it. If now the stiffness of the cochlear partition were doubled, then it would respond to this double pressure discontinuity exactly as the natural partition would respond to the single pressure discontinuity of p which would be present if the scala tympani had been drained.

Similarly, where the inertia of the cochlear partition is taken into account (as becomes necessary near the point of resonance) an identical argument shows that a complete cochlea with the partition's inertia as well as its stiffness doubled (or, more generally, with its entire impedance doubled) would respond exactly like the natural cochlea with the scala tympani drained. As has previously been suggested, these are modest changes: although they do reduce somewhat the time taken for a signal to reach a given point of the cochlea, they do not alter the characteristic frequency at that point.

Appendix B. Dispersion in the cochlea

This appendix is concerned to review experimental data, obtained (Rhode 1971) by use of the Mössbauer technique, in the light of the physics of dispersion and group velocity. It also seeks to clarify further the distinction between classical waveguide resonance and critical-layer absorption given in §§ 3 and 4.

Rhode's data were obtained in live squirrel monkeys. He developed a surgical technique whereby a small Mössbauer source† could be placed on the basilar membrane and the cochlea could then be restored to its normal condition. Another Mössbauer source was placed on the umbo of the eardrum; that is, on the point of the tympanic membrane in direct contact with the handle of the malleus. Accordingly, when the ear was stimulated by an acoustic pure tone, the sinusoidal vibrations of both the basilar membrane and the malleus could be determined in both amplitude and phase.

It is the amplitude *ratios* and phase *differences* that are significant. Thus, if the displacements of the two sources are

$$a_M \cos(\omega t + \theta_M) \quad \text{and} \quad a_B \cos(\omega t + \theta_B) \tag{B 1}$$

for the malleus and basilar membrane respectively, Rhode plots the amplitude ratio and phase difference

$$a_r = a_B/a_M \quad \text{and} \quad \theta_d = \theta_B - \theta_M \tag{B 2}$$

as functions of the frequency in hertz, $\omega/2\pi$.

Figures 8 and 9 show plots of a_r and θ_d against frequency for one particular animal. In common with all of Rhode's phase data it shows that the value of θ_d extrapolated to zero frequency is close to $\frac{1}{2}\pi$. This can be interpreted as follows.

The basilar-membrane displacement at low frequencies is expected to be in phase with the 'slow-wave' pressure p (half the pressure difference across the cochlea partition). Furthermore, a limiting phase difference for low frequency should represent phase difference *at the base*, since for low enough frequency a travelling wave should

† The Mössbauer source, when at rest, emits gamma rays of extraordinarily precise frequency. Accordingly, very small motions of the source can be detected by the Doppler shift they produce. For details of the method, and for important checks on the accuracy of the results, see Rhode (1971).

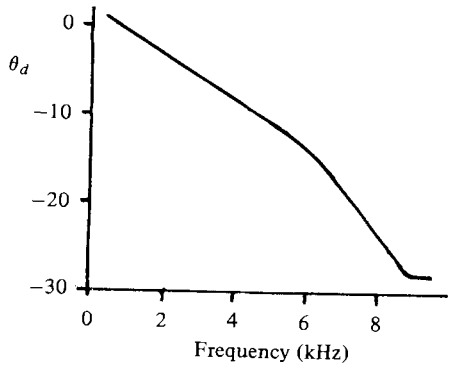

FIGURE 8. Phase difference θ_d in radians between displacements of basilar membrane and of malleus, measured as a function of frequency in kHz by Rhode (1971) in animal 69.662. (Sound intensity 85 dB used near resonant frequency.)

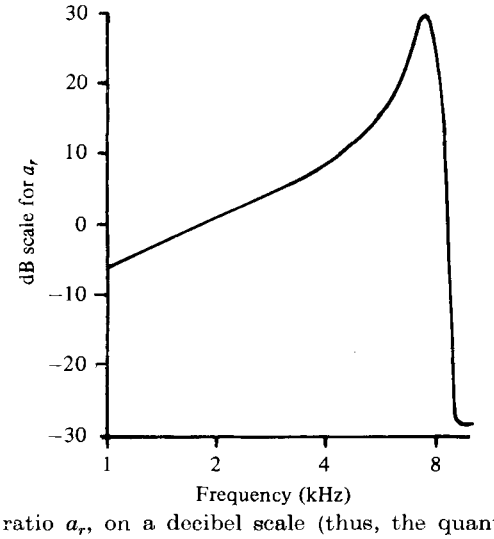

FIGURE 9. Amplitude ratio a_r, on a decibel scale (thus, the quantity plotted is $20 \log_{10} a_r$), measured as a function of frequency in kHz (also shown on a logarithmic scale) by Rhode (1971) in animal 69.473. (Sound intensity 70 dB used near resonant frequency.)

suffer little phase change in the distance (of order 10 mm) between the base and the Mössbauer source. On the other hand, the slow-wave impedance should determine a slow-wave pressure p at the base in phase with stapes velocity (and so with malleus velocity).

Finally, then, the basilar-membrane displacement, being in phase with p, and so with malleus velocity, should have a phase advance of $\frac{1}{2}\pi$ over malleus displacement. Note, too, that this interpretation is supported by the observed low-frequency proportionality of the amplitude ratio a_r to frequency ω (corresponding to a slope of 6dB per octave on a log–log plot such as figure 9).

As frequency increases, however, the phase lag associated with propagation of the travelling wave between the base and the Mössbauer source must gradually overcome the initial phase lead. In fact, as figure 8 shows, the measured phase difference θ_d is

negative at frequencies above about 1 kHz. Furthermore, the phase deficiency $(-\theta_d)$ increases steadily with frequency, in agreement with a travelling-wave interpretation, until the resonant frequency at the position of the source (a frequency around 7–9 kHz in each case studied) is reached. The maximum value of $(-\theta_d)$, reached at the resonant frequency, was found to lie between 20 and 30 radians in every case.

Strictly speaking, the expressions (B 1) and (B 2) define θ_d only to within an arbitrary number of whole rotations (integer multiples of 2π). Nevertheless, the measured low-frequency value $\frac{1}{2}\pi$ has a clear physical interpretation as we have seen, and the variation as ω increases was found to be smooth and continuous (nothing is observed that can be interpreted as a jump by 2π). It follows that the difference between $\frac{1}{2}\pi$ and the value of θ_d so determined (falling to a limiting value of between -20 and -30) can be taken as indicating the true phase lag in the travelling wave between the base and the Mössbauer source at frequencies below the resonant frequency.

By contrast, the measurements above the resonant frequency are characterized by a constant phase difference θ_d. In this region, indeed, basilar-membrane displacement is either exactly in phase or (more commonly) exactly in antiphase with malleus displacement; an observation which appendix A tentatively interprets as a response of the basilar membrane to a standing-wave distribution of the fast-wave pressures P, following on a complete extinction of the travelling slow wave p.

Now, we have seen that Rhode's method of deriving θ_d (plotting the phase difference as a continuous function of frequency) is specially appropriate at frequencies where the travelling wave is present. On the other hand, when applied at higher frequencies to a basilar-membrane displacement in exact phase or antiphase with malleus displacement, it necessarily gives θ_d a rather arbitrary value as the even or odd multiple of π closest to the value just below the resonant frequency. For a value between -20 and -30 this is in practice either -7π, -8π or -9π; the values quoted by Rhode as observed in every case.

The remainder of this appendix is concerned with frequencies below the resonant frequency, where the travelling slow wave is dominant. If that wave, at all positions between the base and the Mössbauer source, were *non-dispersive* (that is, if its speed had a value independent of frequency), then the time of travel of the slow wave between those points (say, τ) would be similarly constant; and the phase lag would be

$$\tfrac{1}{2}\pi - \theta_d = \omega\tau. \tag{B 3}$$

Equation (B 3) represents a straight line on the plot of θ_d against ω; a line whose slope gives the time of travel τ.

Figure 8 shows that, below about 5 kHz, the measured phases lie on such a straight line; this is consistent with the assumption of a non-dispersive travelling wave. The associated travel time is 0·40 ms, corresponding to a *mean* wave speed of 40 m s^{-1} in the 16 mm between the base and the source.†

By contrast, the departure from a straight line above about 5 kHz is very marked. Similar behaviour is found in Rhode's other experiments. This proves that, above about 5 kHz, the travelling wave is dispersive *somewhere* between the base and the source.

A crude estimate of the travel time τ from equation (B 3) would show it increasing

† This may be compared (see later) with an estimated low-frequency wave speed of 15 m s^{-1} *at* the source itself.

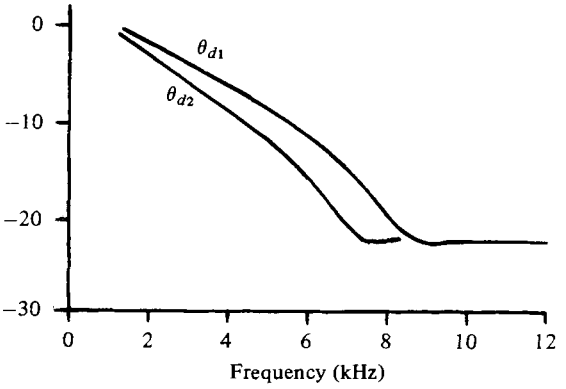

FIGURE 10. Phase differences θ_{d1} and θ_{d2} measured as in figure 8 at two points 1 and 2 on the basilar membrane (1·5 mm apart) in animal 69.434.

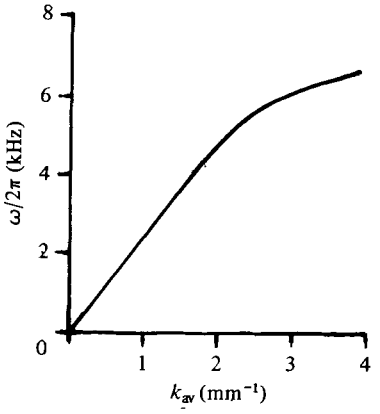

FIGURE 11. Average wavenumber k_{av} between points 1 and 2, deduced from results in figure 10 by equation (B 4), and plotted as abscissa against frequency $\omega/2\pi$ (in kHz) as ordinate.

from 0·40 ms to 0·53 ms between 5 and 9 kHz. It must be emphasized, however, that this is only a travel time *for wave crests*.

From the standpoint of energy flow, on the other hand, it is known that dispersive waves for which the speed of wave crests shows such a *decrease* with increasing frequency have the property that the wave energy travels at a still slower speed: the group velocity. Two features of Rhode's measurements help to indicate the magnitude of this difference.

One clue is given by Rhode's indirect information about wavenumber. The wavenumber, k, in a travelling wave was defined in § 4 as the rate of decrease of phase with distance of travel;† which, fortunately, can be estimated from Rhode's two-source experiments.

Thus, figure 10 is a plot against frequency of both θ_{d1} and θ_{d2}, the measured values

† Note that there is no possibility of giving wavenumber the very simple definition, 2π divided by wavelength, if the wave speed varies with position (as it does in the cochlea, decreasing towards the apex); that, indeed, would make such a definition inapplicable whether or not there is also dispersion (variation of wave speed with frequency).

of θ_d at two positions (1·5 mm apart) where two different Mössbauer sources (1 and 2, each of size 0·06 mm) had been placed. Now, the above definition of the wavenumber k implies that its *average value* k_{av} in the region between the two sources is given by the divided difference

$$k_{\mathrm{av}} = (\theta_{d1} - \theta_{d2})/(1{\cdot}5 \text{ mm}); \tag{B 4}$$

and that this expression should hold throughout that range of frequencies (up to 7 kHz) for which the measurements suggest that a travelling wave remained dominant at position 1 (as well as at position 2).

Roughly, we may take k_{av} as indicating a value of k halfway between the two sources. Figure 11 plots k_{av} as the abscissa against ω as the ordinate, to give a presentation similar to that of figure 5.

In such a plot, ω is the rate of change of phase with time, and k its rate of change with distance. Thus, their ratio ω/k is the speed of travel of wave crests. Figure 11 confirms the earlier indication that this speed is independent of frequency (the wave is non-dispersive) below about 5 kHz. In this frequency range, the ratio ω/k_{av} (value taken by that speed halfway between the two sources) is 15 m s^{-1}.

Above 5 kHz, however, figure 11 indicates a very clear flattening of the graph of ω against k_{av}. The speed ω/k_{av} of wavecrests falls from 15 m s^{-1} to 10 m s^{-1}; a significant reduction.

From the standpoint of energy flow, however, it is much more important that the *slope* of the curve in figure 11 falls from 15 m s^{-1} to 3 m s^{-1}: a fivefold reduction. This slope of a graph of frequency ω against wavenumber k is, of course, the group velocity, U; that is, the velocity of energy propagation. (For the extremely well-established foundations of this century-old principle, see any textbook of wave physics.) Fortunately, in the present case, Rhode's own data afford another check on the fivefold reduction in energy propagation velocity that the result implies.

To see this, note that the slow-wave impedance at the base determines the power input P into the travelling wave as proportioned to stapes velocity squared, and hence to malleus velocity squared, $(\omega a_M)^2$. On the other hand, the wave energy per unit length, E, is necessarily twice the potential energy (as in any vibrating system), which in turn is proportional to basilar-membrane displacement squared, a_B^2. Thus, the ratio P/E is proportional to

$$(\omega a_M)^2/a_B^2 = \omega^2/a_r^2 \tag{B 5}$$

in terms of the amplitude ratio (B 2).

That ratio P/E is an *upper bound* to the group velocity U. This is because the power transmitted by the wave is EU (energy per unit length times energy propagation velocity); which, in turn, must be equal to the power input P if negligible energy dissipation has occurred, and can only become *less* than P as a result of energy dissipation.

We have seen that, at low frequencies, the waves are non-dispersive, with $U = 15$ m s^{-1}; in this frequency range, too, they are non-dissipative, so that P/E must have the same value at those frequencies. Figure 9 confirms that P/E, proportional by (B 5) to ω^2/a_r^2, is indeed constant at low frequencies, as is evident from the slope of 6 dB per octave (on a log–log plot of a_r against frequency) already mentioned.

From the known low-frequency value 15 m s^{-1} for P/E, from its proportionality to ω^2/a_r^2, and from the values of a_r in figure 9, we derive values of P/E as in figure 12.

Remembering that P/E is an *upper bound* to U, we have here (and from similar results for other animals) a confirmation that the energy propagation velocity U suffers at least a fivefold reduction.

Neither of the two methods by which this result has been obtained would allow us to identify any further reductions in U which may be present. For example, this last method could not indicate them because of the rapidly growing importance of dissipation as the resonant frequency is approached.

Similarly, large dissipation must reduce the efficacy of the former method. That is because, as the travelling slow wave becomes more and more damped, the signal becomes dominated more and more by the *residual* wave of fixed amplitude and phase (the one interpreted in appendix A as a standing fast wave). This must artificially bring to a halt the normal travelling-wave increase in the phase deficiency $(-\theta_d)$, and so also in k_{av}; and, therefore, restrict the extent of any increase in the slope U of ω against k_{av}.

Nevertheless, it is interesting to pursue from a theoretical standpoint the strong possibility that the local value of k at a given point may continue to increase without limit as ω approaches the resonant frequency ω_r at that point. Suppose, for example, that k increases in proportion to

$$(\omega_r-\omega)^{-N}, \tag{B 6}$$

where $N > 0$. Then differentiation shows that $dk/d\omega$ increases in proportion to

$$(\omega_r-\omega)^{-N-1}; \tag{B 7}$$

therefore, the slope $U = d\omega/dk$ of the graph of ω against k decreases in proportion to

$$(\omega_r-\omega)^{N+1}, \tag{B 8}$$

which is necessarily faster than $(\omega_r-\omega)$ itself, as suggested in figure 1 (*b*).

These conclusions at a fixed *position* imply some even more interesting conclusions for energy flow at a fixed *frequency* ω. At a distance x from the base just a little less than its value x_r at the point where ω is the resonant frequency, the local resonant frequency ω_r must *exceed* ω by a small amount $(\omega_r-\omega)$ closely proportional to (x_r-x). Thus, by (B 8), the velocity of energy propagation U must be proportional to

$$(x_r-x)^{N+1}, \tag{B 9}$$

where $N > 0$. Therefore, the time $\int dx/U$ for the energy at frequency ω to travel a distance x is proportional to

$$\int \frac{dx}{(x_r-x)^{N+1}} = \text{constant} + \frac{1}{N(x_r-x)^N}, \tag{B 10}$$

which increases without limit as x approaches x_r.

This unlimited time available represents, of course, the fundamental feature of critical-layer absorption. Essentially, it allows any damping rate, however weak, to dissipate all the energy without reflection.

By contrast, classical waveguide resonance requires k to tend to zero, at a fixed position, as ω tends to ω_r *from above* (so that the energy propagation velocity U can remain positive). If k is proportional to

$$(\omega-\omega_r)^n \tag{B 11}$$

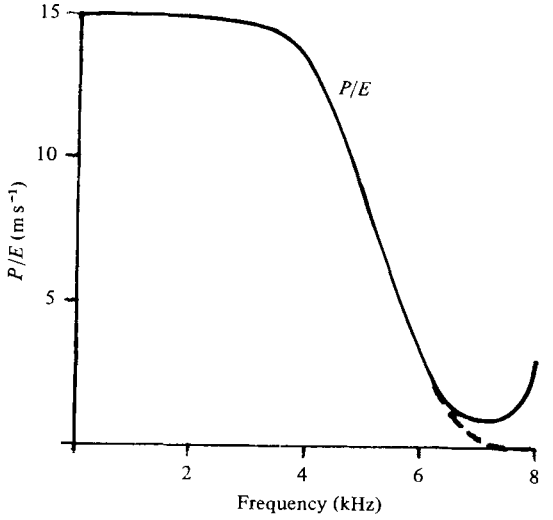

FIGURE 12. Plain line: ratio of power input P to energy flow E, deduced as explained in the text from the values of a_r plotted in figure 9 for Rhode's animal 69.662. These results show a thirtyfold reduction in P/E. When measurements in other animals under other conditions are used, the corresponding reduction in P/E is typically by a smaller factor than 30, but in no case is it by a factor of less than 5. This confirms that the group velocity U (which is equal to P/E at low frequency, and must fall below it near resonance, as a result of energy dissipation) suffers at least a fivefold reduction. The results, furthermore, are consistent with the possibility that the group velocity actually falls to zero at resonance, as indicated by the broken line.

with $n > 0$, then $dk/d\omega$ is proportional to

$$(\omega - \omega_r)^{n-1} \tag{B 12}$$

and U is proportional to

$$(\omega - \omega_r)^{1-n}. \tag{B 13}$$

If $0 < n < 1$, this does tend to zero, although considerably more slowly than $(\omega - \omega_r)$ itself, as suggested in figure 1 (*a*).

For fixed frequency ω, again, such a classical waveguide resonance would make U proportional to

$$(x_r - x)^{1-n}, \tag{B 14}$$

with $n > 0$. Then the time $\int dx/U$ for the energy to travel a distance x is proportional to

$$\int \frac{dx}{(x_r - x)^{1-n}} = \text{constant} - \frac{1}{n}(x_r - x)^n, \tag{B 15}$$

which remains finite as x approaches x_r. In such a case, reflection of wave energy can occur, with only a limited time available for any action of damping. The above highly contrasted behaviour in the two types of travelling-wave systems with resonance was used in §§ 3 and 4 to strengthen the conclusion that energy flow in the cochlea must be dominated by critical-layer absorption.

Appendix C. One-dimensional models

The general nature of one-dimensional models of the slow wave is described at the beginning of § 5; while, in appendix A, the appropriate equations (A 8) are derived for a particular limiting case. This is the case when only the *stiffness* of the cochlear partition determines its motion in response to the difference between the pressure $P+p$ (taken as uniform over a cross-section of the scala vestibuli) and the pressure $P-p$ (taken as uniform over a cross-section of the scala tympani).

Although such a model cannot exhibit any resonance, or (indeed) any dispersion, it has two important uses. At low enough frequencies (of the order of 100 Hz or less) it may be applied, with a boundary condition to represent the properties of the helicotrema (see below), so as to describe the motions throughout the cochlea; whereas, at those higher frequencies which exhibit resonance at a particular place in the cochlea, the stiffness-dominated model may still have adequate accuracy in certain other parts of the cochlea; namely, those parts which are substantially closer to the base than the position of resonance.

Close to the base, in fact, the cochlear partition has its greatest stiffness; or, in the language of appendix A, its least distensibility D; defined as the proportional increase in the cross-sectional area A of (say) the scala vestibuli per unit excess of pressure in that scala over that in the scale tympani. Nevertheless, in considering equations (A 8), we have observed that even this minimum value of D is so much greater than the compressibility of the fluid that compressibility can be completely neglected. (It must be at least two orders of magnitude less than D because the slow-wave speed (A 10) is at least one order of magnitude less than the sound speed (A 9).) Rewriting (A 8) with K omitted, and dropping the suffix zero from the effectively constant density ρ of the fluid, we obtain

$$\rho\,\partial j/\partial t = -A\,\partial p/\partial x, \quad -\partial j/\partial x = 2AD\,\partial p/\partial t \tag{C 1}$$

as the equations governing the variation of excess volume flow j and pressure p in the stiffness-dominated slow wave.

Equations (C 1) with j eliminated give

$$A\frac{\partial^2 p}{\partial t^2} = c^2\frac{\partial}{\partial x}\left(A\frac{\partial p}{\partial x}\right), \quad \text{where} \quad c = (2\rho D)^{-\frac{1}{2}}, \tag{C 2}$$

the latter expression being the slow-wave speed (A 11). Superficially, equation (C 2) for p is identical with the fast-wave equation for P except in so far as the sound speed c_0 is replaced by the slow-wave speed c. However, the degree of variability of coefficients is extremely different in the two cases: the fast wave speed c_0 is constant, so that the only variable coefficient in (A 13) is A which decreases by a factor of little more than 2 from base to apex. The same variable coefficient A is, admittedly, present in (C 2), but its variability is swamped by that of the slow-wave speed c, which decreases by practically two orders of magnitude from base to apex.

There are two possible methods of treatment of an equation such as (C 2). One is an approximate method, based physically on the idea of energy flow, together with an assumption that variation in physical properties along the cochlea is sufficiently smooth and gradual to avoid backscatter of energy. This is equivalent, as we shall verify, to the mathematical approach known as WKB. The second method is to use

an exact analytical or numerical solution; the first such solution to have been found, due to Zwislocki (1948), is still a most helpful one, and is used below to map out the region of accuracy of an energy-flow (otherwise, WKB) solution.

There is, of course, special interest in travelling-wave solutions of (C 2). The energy-flow method views these as follows.

Equation (C 2) represents a non-dispersive wave system with the wave speed c independent of frequency, so that both the wave crests and also the wave energy travel at speed c. The time to travel a distance x from the base $x = 0$ is

$$\int_0^x c^{-1} dx. \tag{C 3}$$

A wave travelling in the direction x increasing is expected, therefore, to have the form

$$p = f(x) \exp\left[i\omega\left(t - \int_0^x c^{-1} dx\right)\right], \tag{C 4}$$

where the real function $f(x)$ represents its amplitude.

Here, the wave energy per unit length is

$$AD[f(x)]^2. \tag{C 5}$$

To see this, note that the definition of the distensibility D makes the *volume displacement* per unit length (that is, the change in cross-section of the scala vestibuli) ADp. The pressure difference which generated that volume displacement has changed from its undisturbed value 0 to its present value of $2p$, with an average of p. The potential energy (work done by that pressure difference) per unit length is the product of ADp with p. Its average over a cycle is one-half of (C 5). But in any vibrating system the average kinetic and potential energies are equal; a consideration which raises the total wave energy per unit length to the value (C 5).

The wave-energy flow is equal to the energy per unit length (C 5) times the energy propagation velocity c; thus, it is

$$cAD[f(x)]^2 = A[f(x)]^2/2\rho c, \tag{C 6}$$

where D is substituted for as $1/2\rho c^2$ from (C 2). In a travelling wave without dissipation, energy flow must be constant, so that the amplitude $f(x)$ of pressure fluctuations must vary with position in proportion to

$$(c/A)^{\frac{1}{2}}. \tag{C 7}$$

This clear physical method of deriving amplitude variation gives the same result as the asymptotic method known as WKB. In that method, a solution

$$p = f(x) \exp[i\omega(t - g(x))] \tag{C 8}$$

is substituted in the differential equation (C 2) to give

$$-\omega^2 A f c^{-2} = (Af')' - i\omega[(Ag')'f + 2Ag'f'] - \omega^2 Ag'^2 f. \tag{C 9}$$

In the asymptotic limit of high frequency ω, equation (C 9) will be closely enough satisfied if (i) the terms in ω^2 balance, giving

$$g'^2 = c^{-2} \quad \text{so that} \quad g = \int_0^x c^{-1} dx \tag{C 10}$$

exactly as in (C 4); and (ii) the terms in ω balance, giving

$$f'/f = -\tfrac{1}{2}(Ag')'/(Ag'), \tag{C 11}$$

so that f is proportional to

$$(Ag')^{-\frac{1}{2}} = (c/A)^{\frac{1}{2}}, \tag{C 12}$$

exactly as in (C 7). The first term on the right-hand side of (C 9), independent of ω, should be insignificant compared with the terms in ω and ω^2 at high enough frequency.

There are various good ways for estimating how high the frequency needs to be for the convenient WKB expression (C 4), with $f(x)$ given by (C 7), to be a closely accurate solution of equation (C 2). However, the most clearly convincing approach to this equation, in the context of cochlear mechanics, is by comparing exact solutions, for distributions of c and A close to those in a real cochlea, with the corresponding WKB solutions.

An exact solution very useful for this purpose is that given by Zwislocki (1948) for the case

$$c = c_b \exp(-\alpha x), \quad A = A_b, \tag{C 13}$$

where c_b and A_b are the values of c and A at the base $x = 0$. Equations (C 13) readily allow for a distribution of c which varies, as in the real cochlea, by practically two orders of magnitude (while the distensibility, according to (C 2), would vary like $\exp(2\alpha x)$ by practically four orders of magnitude). It should be much less relevant to questions about the accuracy of a WKB solution that the real cross-sectional area A shows a far more gradual variation, by a factor of little more than 2; therefore, for comparison purposes, it is sufficient to make use of an exact solution for a system with constant A.

Equations (C 13) substituted in (C 2) give a solution

$$p = F(x)\exp(i\omega t), \quad \text{where} \quad F''(x) + \omega^2 c_b^{-2} F(x)\exp(2\alpha x) = 0. \tag{C 14}$$

Here, comparison with the approximate form (C 4) reminds us that we must expect $F(x)$ to be complex, representing the variation with x not only of amplitude but also of phase.

In equation (C 14) the substitution

$$Z = \omega c_b^{-1}\alpha^{-1}\exp(\alpha x), \quad d/dx = \alpha Z\, d/dZ \tag{C 15}$$

produces a reduction to Bessel's equation

$$(Z\,d/dZ)(Z\,dF/dZ) + Z^2F = 0, \tag{C 16}$$

with its two independent real solutions $J_0(Z)$ and $Y_0(Z)$, the well-known Bessel functions. On the other hand, to represent how a wave, travelling in the direction x increasing, is generated at the base $x = 0$, it is necessary to use a complex linear combination of these two solutions,

$$F = H_0^{(2)}(Z) = J_0(Z) - iY_0(Z). \tag{C 17}$$

Indeed, the known asymptotic form of (C 17) for large Z,

$$H_0^{(2)}(Z) \sim \left(\frac{2}{\pi Z}\right)^{\frac{1}{2}} e^{-i(Z-\frac{1}{4}\pi)}\left(1 + \frac{i}{8Z} - \frac{9}{128Z^2} + \ldots\right), \tag{C 18}$$

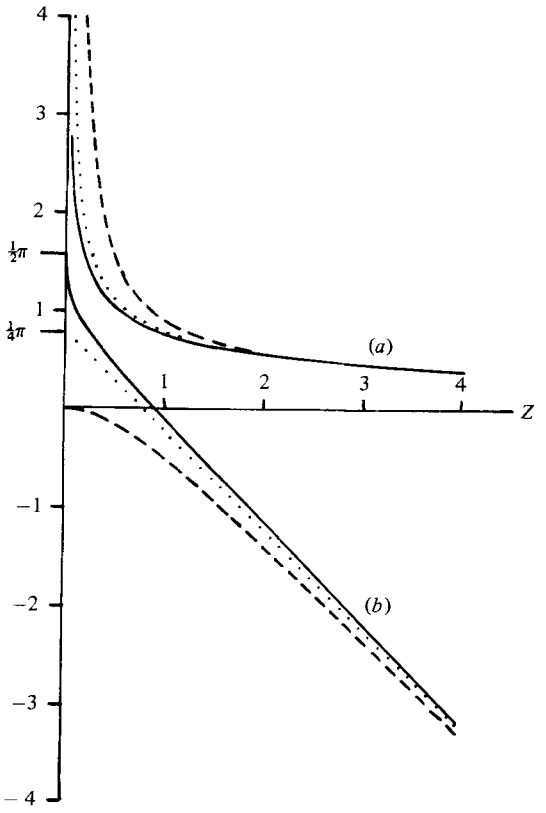

FIGURE 13. Stiffness-dominated solution of Zwislocki (1948) for pressure (plain line) and volume flow (broken line), compared with their common form (dotted line) on the WKB approximation: (*a*) amplitudes; (*b*) phases. ——, F; – – –, (idF/dZ); · · · · ·, $(2/\pi Z)^{\frac{1}{2}}\, e^{-i(Z-\frac{1}{4}\pi)}$.

shows it to possess the necessary travelling-wave property (frequently described as 'the radiation condition'); specifically, its phase *decreases* with increasing x. By contrast, any combination of J_0 and Y_0 in different proportions would include a component whose phase increases with x for large x, representing a wave travelling in the direction x decreasing with a flow of energy inward 'from $x = +\infty$'.

It will be noted that expressions (C 13) and (C 15) for c and Z make

$$\omega \int_0^x c^{-1} dx = \omega c_b^{-1} \alpha^{-1} [\exp(\alpha x) - 1] = Z - \omega c_b^{-1} \alpha^{-1}; \tag{C 19}$$

therefore, the leading term in the asymptotic expression (C 18) is consistent with the phase behaviour (C 4) given on the WKB approximation. Equally, its amplitude is proportional to $Z^{-\frac{1}{2}}$ and therefore to $c^{\frac{1}{2}}$, just as the WKB approximation (C 7) predicts. Numerically, these asymptotic forms become quite good approximations for $Z > 1{\cdot}5$, as the asymptotic series in (C 18) already suggests. This is confirmed by figure 13, which plots amplitude and phase of the solution (C 17) for comparison with the WKB approximate forms derived from the leading term in the asymptotic expansion (C 18).

The condition $Z > 1{\cdot}5$ for good accuracy of the WKB approximation can be conveniently expressed in terms of the wavenumber

$$k = \omega c^{-1} = \omega c_b^{-1} \exp(\alpha x) \tag{C 20}$$

as a condition $k > 1{\cdot}5\alpha$. The largest possible value of α is $[\ln(100)]/(35\text{ mm})$, corresponding to four orders of magnitude increase in distensibility along a cochlea of 35 mm length. Therefore it may be assumed that the WKB approximation is accurate wherever

$$k > 1{\cdot}5[\ln(100)]/(35\text{ mm}) = 0{\cdot}2\text{ mm}^{-1}. \tag{C 21}$$

Furthermore, it is reasonable to use this condition for energy flow without backscatter, $k > 1{\cdot}5\alpha$, relating k to the proportional rate of variation, α, of a steeply varying quantity c with distance along the cochlea, even though some *other* property such as the cross-sectional area A is also varying; at least, if it has a much lower proportional rate of variation (as is, indeed, the case).

Most of what follows will be concerned with applications of the WKB method in regions where the inequality (C 21) is satisfied. First of all, however, the exact solution (C 17) is used to give some suggestions about behaviour in conditions where (C 21) is not satisfied.

In a position such as the first cochlear bend of the squirrel monkey, where Rhode's data outlined in appendix B were gathered, the wave speed c is about 15 m s^{-1}. Therefore, the condition $k > 0{\cdot}2\text{ mm}^{-1}$ for energy flow without backscatter requires that $\omega = kc > 3000\text{ s}^{-1}$, or $\omega/2\pi > 500$ Hz. In fact, this condition was satisfied for almost all of Rhode's data points.

Nearer the apex, the lower limit on frequency for the WKB approximation to be applicable must decrease rather steeply (in proportion to c) until, at the apex itself, no acoustically interesting frequencies are excluded. This consideration is found to be important later, when the influence of the helicotrema is treated.

Nearer the *base*, however, the lower limit on frequency for use of WKB must increase to 1 kHz or a little more. This implies that at frequencies below 1 kHz there is necessarily a region near the base where the WKB approximation has impaired accuracy. Fortunately, in this proximal region the cross-sectional area A varies little, so that it is specially appropriate to use Zwislocki's exact solution for the case (C 13). Then the asymptotic property (C 18) can be applied, as Steele & Taber (1979*a*, *b*) pointed out, to match that solution to the WKB approximation employed in the rest of the cochlea.

In this context, it is useful to calculate the excess volume flow j corresponding to the Zwislocki solution (C 14). By the first of equations (C 1) it is

$$j = -(\rho i\omega)^{-1} A(dF/dx)\exp(i\omega t), \tag{C 22}$$

depending on the gradient of $F(x)$. Using (C 15), with (C 13), we can write this as

$$j = (A/\rho c)(i\,dF/dZ)\exp(i\omega t). \tag{C 23}$$

The first factor in (C 23) represents the standard form $(A/\rho c)$ for the 'admittance' (reciprocal of the impedance) of a one-dimensional wave in a tube of cross-section A and wave speed c. In the region $Z > 1{\cdot}5$ where the WKB approximation is good, the solution (C 17) has $(i\,dF/dZ)$ very close to F, as the asymptotic form (C 18) suggests

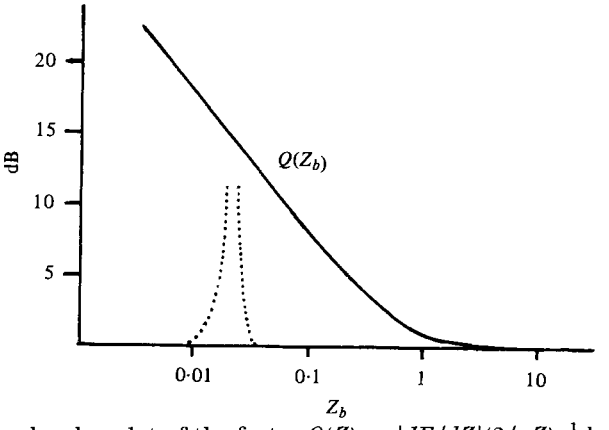

FIGURE 14. Plain line: log–log plot of the factor $Q(Z) = |dF/dZ|(2/\pi Z)^{-\frac{1}{2}}$ by which the broken line in figure 13(*a*) exceeds the dotted line. The ordinate is $20 \log_{10} Q(Z_b)$, representing in decibels, as a function of $Z_b = \omega c_b^{-1} \alpha^{-1}$, *either* (i) the additional sound level required to produce a given energy flow in the travelling wave; *or* (ii) a reduction in travelling-wave amplitudes generated by given footplate vibration. Dotted line: mitigation of this reduction produced (see below) at low frequencies by helicotrema resonance.

and figure 13 verifies. In that region, then, the volume flow and pressure are practically in phase and their ratio is this standard slow-wave admittance $(A/\rho c)$.

For $Z < 1{\cdot}5$ there is, as figure 13 indicates, some departure of $i\,dF/dZ$ from F both in amplitude and phase. This has several implications, as follows.

At the base value of Z,

$$Z = Z_b = \omega c_b^{-1} \alpha^{-1}, \tag{C 24}$$

the fact that the pressure is *not perfectly in phase with volume flow* reduces the power of any given vibration of the stapes footplate to feed energy into the slow wave. Figure 13 shows that, as Z_b decreases, the phase difference between pressure and volume flow increases from 0 to an ultimate limit of $\frac{1}{2}\pi$ at $Z_b = 0$. The travelling-wave solution in this zero-frequency limit has pressure in quadrature with volume flow, so that no energy at all can be fed into the slow wave (however, we shall see that at frequencies as low as this a travelling-wave solution ceases to be applicable because of reflection at the apex). At intermediate values of Z_b there is (i) an energy-absorbing component of pressure, in phase with volume flow, and (ii) a component in quadrature, which cannot absorb energy and therefore makes no contribution to generation of a travelling wave.

The amplitude results in figure 13 give a good idea of the extent to which, when $Z_b < 1{\cdot}5$, a given level of energy flow in the travelling wave (as represented by the in-phase pressures and volume flows in the part of the diagram with $Z > 1{\cdot}5$) requires footplate vibrations augmented in amplitude by a certain factor. This is the factor $Q(Z)$ by which, at $Z = Z_b$, the broken line (representing volume flow) exceeds the dotted line (volume flow required according to the WKB approximation). Figure 14 shows that factor on a decibel scale, as a function of Z_b. The quantity plotted can be interpreted *either* as (i) increased sound level required at lower frequencies to produce a given energy flow in the travelling wave; *or* as (ii) reduced power input into the

travelling wave generated by a given vibration of the stapes footplate; *or* as (iii) reduced real part of the input impedance to the cochlea at the oval window.

Appendix B gives a method for analysing data such as those of Rhode (1971) which assumes, among other things, a constant slow-wave input impedance $\rho c_b/A_b$ at the base. Although figure 14 emphasizes that at Rhode's lower frequencies the input impedance is reduced below that assumed value, we may note that the extent of the reduction is too modest to be observable within the scatter of Rhode's low-frequency data.

It might be marginally more feasible, in experiments such as those of Rhode (1971), to observe at lower frequencies a slight departure of the phase difference θ_d from the value (equation (B 3)) which the WKB approximation indicates at lower frequencies. The departure should take the form of an *increase*, by the sum of (i) excess phase of the pressure *at the point of measurement* (full line) over its WKB value (dotted line), and (ii) the deficiency in phase of the volume flow *at the base* $Z = Z_b$ (broken line) below its WKB value (dotted line). Although at the frequencies used the excess phase (i) has already been noted as very small, figure 13 suggests that at the lower frequencies the phase deficiencies (ii) could raise θ_d above the straight line (B 3) by up to $\frac{1}{4}\pi$. In the light of this it is interesting to note that Rhode's phase measurements at his lowest frequencies are indeed seen to lie above that line by a margin of error between 0 and $\frac{1}{4}\pi$.

More generally, we can use figure 13, at any of those frequencies which exhibit resonance at a particular place in the cochlea, to *match a WKB soluiion* to the stapes vibrations that may generate it. This involves noting (at those frequencies) how much, if at all, figure 13 makes the values of pressure and volume flow depart, in the region much nearer to the base than the position of resonance, from values given by the WKB approximation.

A stiffness-dominated one-dimensional model has one other important function: to represent the motions *throughout* the cochlea at those still lower frequencies that fall significantly below *any* resonant frequency in the cochlea. These are frequencies (around 100 Hz or less) for which the slow wave extends all the way to the apex, so that it is necessary to consider what boundary condition determines the reflection, if any, that may occur at the apex.

Careful consideration along these lines leads to a conclusion of definite physiological interest. Although (as noted in appendix A) the fast wave obviously satisfies the condition $J = 0$ at the apex (where termination of the cochlea forces the net volume flow to be zero), the corresponding condition on the slow wave is different: non-zero volume flows $+j$ in the scala vestibuli and $-j$ in the scala tympani are possible at the apex provided that an equal volume flow j passes through the helicotrema from the scala vestibuli into the scala tympani.

As is well known, the helicotrema is a small hole in the cochlear partition, of diameter from 0·25 to 0·30 mm, situated very close to the apex. This permits direct movement of perilymph, through the hole, between the scala vestibuli and the scala tympani. The required boundary condition at the apex should relate the volume flow j through the hole to the pressure difference $2p$ which forces it.

From the standpoint of the mechanics of oscillatory flows, the helicotrema is a *constriction*; indeed, its area (about 0·06 mm^2) is an order of magnitude less than the cross-sectional area of the scala vestibuli just proximal to it. The pressure difference

$2p$ across such a constriction has to balance primarily the substantial *acceleration* of fluid as a given volume flow j is channelled through the narrow hole. The required pressure difference for a hole of diameter d is known to be about

$$2p = (\rho/d)\,dj/dt, \tag{C 25}$$

where the quantity in brackets is referred to as the 'inductance' or 'inertance' of the hole (see Lighthill 1978, § 2.5, for methods of calculating this). In addition to this inertial term (C 25) in $2p$, there is also a viscous-resistance term directly proportional to j; but consideration of its damping effect may, at this stage, be usefully postponed.

In the apical portion of the cochlea, where the WKB approximation can be used even at frequencies of the order of 100 Hz, we may take the pressure as

$$p = T(c/c_b)^{\frac{1}{2}}(A_b/A)^{\frac{1}{2}}\left\{\exp\left[i\omega\left(t-\int_0^x c^{-1}dx\right)\right]\right.$$
$$\left.+R\exp\left[i\omega\left(t-\int_0^L c^{-1}dx-\int_x^L c^{-1}dx\right)\right]\right\}. \tag{C 26}$$

Here, the first line represents a forward travelling wave which satisfies the WKB relationship (C 12) and which, when extrapolated to the base according to that relationship, would have amplitude T; while, of course, figure 13(a) indicates how the true amplitude near the base would fall short, by the factor by which the full line falls below the dotted line.

The second line in (C 26) represents, on exactly the same basis,† the wave reflected at the apex $x = L$ (where L is the length of the cochlea, measured along its helically curved axis). In this line, the first integral represents the time taken for the wave to reach $x = L$, and the second integral the time for its reflection to reach the point with co-ordinate x. The coefficient R may be complex, with an argument representing a phase change due to the presence of the helicotrema. On the other hand, while damping is still not taken into account, there can be no amplitude change and we must expect that $|R| = 1$.

The corresponding WKB approximation to j is obtained by multiplying by the local slow-wave admittance $(A/\rho c)$, as discussed after equation (C 23); and, also, changing the sign in the second line, because it is the volume flow *in the direction of propagation* that is in phase with p. Thus,

$$j = T(A/\rho c)(c/c_b)^{\frac{1}{2}}(A_b/A)^{\frac{1}{2}}\left\{\exp\left[i\omega\left(t-\int_0^x c^{-1}dx\right)\right]\right.$$
$$\left.-R\exp\left[i\omega\left(t-\int_0^L c^{-1}dx-\int_x^L c^{-1}dx\right)\right]\right\}. \tag{C 27}$$

The reflection coefficient R can now be determined by applying the boundary condition (C 25) to the values of (C 26) and (C 27) at the apex $x = L$. Suppressing factors which appear on both sides of the resulting equation, we obtain

$$2(1+R) = (A_a/c_a d)\,i\omega(1-R), \tag{C 28}$$

† Note that this corresponds to the solution $g' = -c^{-1}$ of (C 10); also, (C 17) must be replaced by its complex conjugate $H_0^{(1)}(Z) = J_0(Z) + iY_0(Z)$; so that the amplitude modifications near the apex in figure 13 are retained but the phase modifications have their sign changed.

where subscript a denotes values at the apex. The solution of (C 28) for R does, as expected, have $|R| = 1$ and can, if desired, be expressed as a phase advance in the reflected wave:

$$R = [1 + (2ic_a d/A_a\omega)]/[1 - (2ic_a d/A_a\omega)] = \exp[2i\tan^{-1}(2c_a d/A_a\omega)]. \quad \text{(C 29)}$$

The fact that a constriction leads to such a phase advance in a reflected wave is a well-known general property of one-dimensional waves in fluids (Lighthill 1978, p. 120). Its application here leads to an interesting suggestion regarding the helicotrema's function.

Before going into quantitative details, we note the essential idea. The total phase lag as the wave travels from base to apex and its reflection then travels from apex to base can, at one particular frequency, be exactly cancelled by the phase advance due to reflection at the helicotrema. There is then *resonance* at this particular frequency, which produces an increased response of the cochlea to given footplate vibrations. We shall see that this particular resonant frequency may have two valuable properties: (i) affording a *further resonance* at a frequency just below the range of frequencies for which any part of the basilar membrane can resonate; (ii) partially counteracting the loss of cochlear response to tones of relatively low frequency indicated (figure 14) by pure travelling-wave theory. To sum up these suggestions, the helicotrema helps to extend downwards the frequency range for useful auditory response.

In a qualitative sense, we are dealing with 'beer-bottle' resonance such as is commonly generated when any wide tube interacts with a constriction. Modifications that result when *two* wide tubes are separated by a constriction, *and* by a variably distensible partition, and the motion is generated by forcing at the end of one tube, are all of merely quantitative significance. .... Actually, the quantity we are most concerned to estimate is a 'response ratio'; namely, the ratio of volume-flow fluctuations near the apex (the region expected to play the main transduction role at these lower frequencies) to the volume-flow fluctuations at the base associated with footplate vibration.

It is convenient to become quantitative in two stages, of which the first gives only an extremely crude estimate of the resonant frequency. This first stage makes the WKB approximation at all points in the cochlea. Then the ratio (apical to basal volume flow) just referred to is given by putting $x = L$ and $x = 0$ in (C 27), yielding

$$(j)_{x=L}/(j)_{x=0} = [(A_a c_b/c_a A_b)^{\frac{1}{2}} \exp(-i\omega\tau)](1-R)/[1 - R\exp(-2i\omega\tau)] \quad \text{(C 30)}$$

as the WKB approximation to the response ratio. Here, the first factor in square brackets is the corresponding travelling-wave value; while τ stands for the travel time

$$\tau = \int_0^L c^{-1}dx \quad \text{(C 31)}$$

of the slow wave down the cochlea's whole length L.

Comparison with (C 29) suggests that helicotrema resonance (making (C 30) infinite) occurs at a certain frequency $\omega = \omega_H$; namely, the frequency for which the total phase lag $2\omega\tau$ due to wave propagation cancels the phase advance $2\tan^{-1}(2c_a d/A_a\omega)$ due

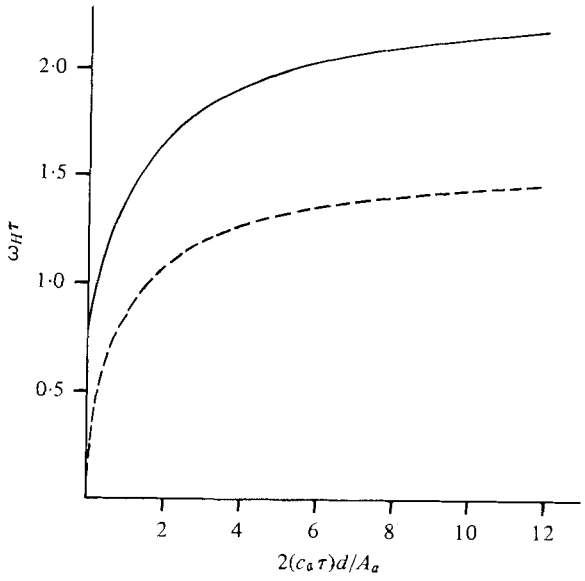

FIGURE 15. The frequency ω_H of helicotrema resonance: dependence of $\omega_H\tau$ on $2(c_a\tau)\,d/A_a$ predicted by the crude approximation (C 32) (broken line) and the improved approximation (C 37) (plain line).

to reflection at the helicotrema. This resonance condition determines ω_H as the frequency for which the one-way phase lag $\omega_H\tau$ satisfies the equation

$$(\omega_H\tau)\tan(\omega_H\tau) = 2(c_a\tau)\,d/A_a. \tag{C 32}$$

Figure 15 (broken line; for full line see later) plots the not very sensitive dependence of $\omega_H\tau$ on $2(c_a\tau)\,d/A_a$ which equation (C 32) predicts.

Just because this dependence is not very sensitive, it should suffice to estimate $(c_a\tau)$ from the simple exponential distribution (C 13) of c, giving by (C 19)

$$c_a\tau = c_a[c_a^{-1}\alpha^{-1} - c_b^{-1}\alpha^{-1}] = \alpha^{-1}(1 - c_a c_b^{-1}) \doteqdot \alpha^{-1} \doteqdot 7{\cdot}5 \text{ mm}, \tag{C 33}$$

where $c_a c_b^{-1}$ is neglected as very small and α is estimated as in (C 21). With an apical cross-section A_a of the scala vestibuli around 0·4 mm^2 and with d about 0·275 mm, this makes the right-hand side of (C 32) equal to about

$$2(7{\cdot}5 \text{ mm})\,(0{\cdot}275 \text{ mm})/(0{\cdot}4 \text{ mm}^2) = 10. \tag{C 34}$$

Figure 15 (broken line) shows that, for any value in the general neighbourhood of 10, the WKB approximation (C 32) makes the one-way phase lag $\omega_H\tau$ close to

$$1{\cdot}4 \text{ radians} = 82 \text{ degrees}. \tag{C 35}$$

This conclusion, however, merely demonstrates what we knew before; namely, the complete lack of realism in the assumption that the WKB approximation is applicable throughout the cochlea. Indeed, (C 35) with (C 33) makes the wavenumber at the apex, $k_a = \omega_H/c_a$, equal to 0·2 mm^{-1}; a value for which the use of WKB at the apex itself is only just acceptable. (We shall see, however, that a more accurate estimate of

ω_H raises k_a to a level which satisfies by a greater margin the condition (C 21) for applicability of WKB.)

The corresponding value of the wavenumber at the base, $k_b = \omega_H/c_b$, is around two orders of magnitude lower, making $Z_b = k_b\alpha^{-1}$ around 0·015. As expected, this is a value for which the WKB approximation is quite seriously in error. Fortunately, however, this is by a rather precisely known margin, shown explicitly in figure 13. Furthermore, its effects on the important response ratio (C 30) are found exclusively in $(j)_{x=0}$, and take a rather simple form, as follows:

(i) *both* in the apically travelling wave and (see footnote above) in the reflected wave, the amplitude of j is increased, by the factor $Q(Z)$ by which the broken line in figure 13(*a*) departs from the dotted line; these changes require us to divide (C 30) by the factor $Q(Z_b)$ already plotted (on a decibel scale) in figure 14;

(ii) the phase lag $\omega\tau$ is decreased where it occurs in the denominator of (C 30) by the margin by which the broken line in figure 13(*b*) departs from the dotted line (again, the footnote explains why the lags are identical in both waves).

Now, in connection with the possibility of helicotrema resonance, it is worth noting that our first crude estimate 0·015 for Z_b is so small as to suggest that the said phase margin is very close to $\frac{1}{4}\pi$. With that value of the phase margin, equation (C 30) would be replaced by

$$(j)_{x=L}/(j)_{x=0} = [(A_a c_b/c_a A_b)^{\frac{1}{2}} \exp(-i\omega\tau)][Q(Z_b)]^{-1}(1-R)\{1-R\exp[-2i(\omega\tau-\tfrac{1}{4}\pi)]\}^{-1}. \tag{C 36}$$

We now determine a revised estimate of the frequency ω_H for helicotrema resonance by equating to zero the expression in curly brackets in (C 36). Furthermore, because the corresponding revised estimate of Z_b turns out to be 0·021, a value of Z for which the relevant phase margin in figure 13(*b*) is very close to $\frac{1}{4}\pi$, it will be unnecessary to make any further revisions in the estimate.

Comparison of (C 29) and (C 36) now shows that helicotrema resonance occurs at the frequency ω_H for which the total phase lag $2(\omega_H\tau - \frac{1}{4}\pi)$ in volume flow cancels the phase advance $2\tan^{-1}(2c_a d/A_a\omega)$ due to reflection at the helicotrema. The equation corresponding to (C 32) then becomes

$$(\omega_H\tau)\tan(\omega_H\tau - \tfrac{1}{4}\pi) = 2(c_a\tau)\,d/A_a. \tag{C 37}$$

Figure 15 (full line) plots the corresponding dependence of $\omega_H\tau$ on $2(c_a\tau)\,d/A_a$.

Once more, this dependence is seen to be relatively insensitive in the neighbourhood of our admittedly rather rough estimate of 10 (see (C 34)) for the right-hand side of (C 37). For any value in the general neighbourhood of 10, equation (C 37) makes $\omega_H\tau$ close to

$$\omega_H\tau = 2{\cdot}1 \text{ radians} = 123 \text{ degrees}. \tag{C 38}$$

With (C 33) this, in turn, makes the wavenumber at the apex, $k_a = \omega_H/c_a$, equal to 0·28 mm^{-1}. This is well within the range (C 21) for which use of the WKB approximation at the apex (which led to (C 29)) is justified. Also, the corresponding wavenumber at the base, $k_b = \omega_H/c_b$, is two orders of magnitude lower, making $Z_b = k_b\alpha^{-1}$ around 0·021. Fortunately, the margin between the broken and dotted lines in figure 13(*b*) differs negligibly from $\frac{1}{4}\pi$ (as assumed above) for values of Z_b of this order.

The dotted line in figure 14 plots, on a decibel scale, the gain in magnitude of the response ratio from the product of the last two factors in (C 36) (that is, the factors

involving R, representing departures from travelling-wave theory). This is plotted as a function of Z_b, with ω and Z_b related as described above. Such a gain, by the amount of the dotted line, is seen to offset significantly the loss (full line) indicated by travelling-wave theory in the same range of values of Z_b. (At higher values, of course, basilar-membrane resonance should play a similar role.)

Here, the dotted-line resonance curve is not extended indefinitely upwards. This is because a significant amount of damping (neglected above) must necessarily accompany helicotrema resonance. The actual extent of viscous damping of flow through the helicotrema cannot be estimated at all precisely without really detailed knowledge of matters such as edge radius of curvature. However, it is easy to see that the helicotrema resonance must be a relatively 'low-Q' system; that is, the resonance peak must have only modest height but substantial bandwidth. Nevertheless, even if damping truncates the resonance peak below the level shown in figure 14, the offset just described is still significant.

The claim that the helicotrema helps to extend downwards the frequency range for useful auditory response by affording an additional resonance (probably of broad bandwidth) below the range of frequencies for which any part of the basilar membrane can resonate is borne out by the value of ω_H calculated above. This is $c_a k_a$ with k_a estimated as $0{\cdot}28\ \mathrm{mm}^{-1}$. The value of the apical slow-wave speed c_a is subject to rather more uncertainty and variability but is of the order of magnitude $1\ \mathrm{m\ s}^{-1}$. There is sufficient indication that the above claim needs to be taken seriously in the fact that the ω_H in hertz corresponding to $c_a = 1\ \mathrm{m\ s}^{-1}$ is 45 Hz.

The rest of this appendix is entirely devoted to those higher frequencies for each of which there is resonance at a particular point of the basilar membrane. This, as discussed in § 1, is a much more lightly damped resonance.

It is emphasized in § 6, and further explained in § 7, that such a resonance is specified (see equation (2)) by a 'stiffness' and an 'inertia'; which, in turn, have to be defined (see equations (3) and (4)) in relation to some particular measure of departure from the undisturbed state called a 'generalized co-ordinate'. Furthermore, a generalized co-ordinate which is extremely convenient both for one-dimensional and multi-dimensional models is noted in § 7 just after equations (3) and (4).

This is V, where $+V$ and $-V$ represent the volume changes in the scala vestibuli and scala tympani per unit length of the cochlea. For this generalized co-ordinate, the *stiffness* s is the ratio $2p/V$, where $2p$ is the pressure difference required to produce the volume change per unit length V. Evidently, the work done by this pressure difference sV in raising the volume change from 0 to V is $\frac{1}{2}sV^2$: the standard form (3) for the potential energy per unit length.

Comparison of the above definition of s with the definition of distensibility given in appendix A and again at the beginning of this appendix shows that

$$s = (AD)^{-1} = 2\rho A^{-1}c^2. \tag{C 39}$$

Here, the second form relates s to the slow-wave speed defined in (C 2).

The corresponding inertia, m, takes a value depending on the shape of the bending mode of the partition in response to a uniform pressure difference. If the volume change V is produced by a partition displacement

$$z = V\zeta(y) \quad \text{across the width} \quad 0 < y < 2l \tag{C 40}$$

of the partition, and the corresponding thickness of the partition is $h(y)$ for $0 < y < 2l$, then the kinetic energy per unit length is

$$\int_0^{2l} \tfrac{1}{2}[\rho h(y)]\,[\dot{V}\zeta(y)]^2\,dy. \tag{C 41}$$

Here, the density of the cochlear partition is taken as indistinguishable from the density ρ of the perilymph, so that $[\rho h(y)]\,dy$ is its mass per unit length between y and $y+dy$; while $\dot{V}\zeta(y)$ is the transverse velocity. By equation (4), the inertia m is the coefficient of $\frac{1}{2}\dot{V}^2$ in (C 41); that is,

$$m = \rho \int_0^{2l} h(y)\,[\zeta(y)]^2\,dy. \tag{C 42}$$

Here, by (C 40), $\zeta(y)$ is the *shape* of the bending mode, normalized so that

$$\int_0^{2l} \zeta(y)\,dy = 1. \tag{C 43}$$

Not surprisingly, with a generalized co-ordinate representing *volume* change per unit length, the inertia per unit length given by (C 42) has the dimensions of *density*.

The expression (C 42) helps to indicate why the partition inertia m may take somewhat larger values than might at first be expected. Thus, it can be rewritten as $(\rho\bar{h}S)/(2l)$, where $\bar{h}$ is a weighted mean of the thickness h with $[\zeta(y)]^2$ as weighting function, and the shape parameter S is $(2l)\int_0^{2l} [\zeta(y)]^2\,dy$. Here, given equation (C 43), S must exceed 1 (because any mean square exceeds the corresponding square of the mean) and can be substantially greater than 1 if the main displacement of the cochlear partition is found within only a small fraction of its overall width. Then m is greater by this large shape factor S than the value, $(\rho\bar{h})/(2l)$, which might be indicated by a very crude argument. The above considerations are part of the case for rejecting the view of Zwislocki (1965) that m must be regarded as negligible.†

In vibrations of the cochlear partition, its rate of change of energy (kinetic plus potential) is equal to the rate $(2p)\,\dot{V}$ of working by the fluid pressure difference $2p$:

$$\partial(\tfrac{1}{2}m\dot{V}^2 + \tfrac{1}{2}sV^2)/\partial t = 2p\dot{V}. \tag{C 44}$$

Divided by $\dot{V}$, this gives

$$m\ddot{V} + sV = 2p, \tag{C 45}$$

the normal equation for a simple harmonic oscillator with natural resonant frequency

$$\omega_r = (s/m)^{\frac{1}{2}} \tag{C 46}$$

(as in equation (2)) subject to an external forcing $2p$.

Now, whatever properties of the cochlear partition are taken into account, the fluid momentum equation remains as in the first of equations (C 1). Also, the downward gradient in volume flow, $(-\partial j/\partial x)$, must represent the local rate of increase $\dot{V}$ in volume per unit length. Therefore, on taking the downward gradient $(-\partial/\partial x)$ of that fluid momentum equation, we obtain

$$\rho\dot{V} = \frac{\partial}{\partial x}\left(A\frac{\partial p}{\partial x}\right). \tag{C 47}$$

† Other parts of the same case are related to the importance of including within m the inertia of all those structures that are mounted on the cochlear partition.

The combined equations (C 45) and (C 47) can be treated in any particular case by numerical methods. It is, however, extremely easy in every case to obtain a solution on the WKB approximation, as follows. This should apply in the cochlea for values of the wavenumber k exceeding a definite limit as in (C 21).

In a travelling wave, the wavenumber k is the rate of decrease of phase (see appendix B just before equation (B 4)). The WKB approximation simplifies the effect of the $\partial/\partial x$ terms in an equation such as (C 47) by assuming that, for large enough k, they act only on the *phase* variation (and not at all on the variation of amplitude, or of a coefficient like A); each $(\partial/\partial x)$, then, is replaced by $(-ik)$. It uses this to define a *dispersion* relationship, and hence an energy propagation velocity; and, finally, as in equations (C 5) to (C 7), determines amplitude variation by conservation of energy flow.

On this programme, (C 47) evidently becomes

$$\rho \ddot{V} = -Ak^2 p, \tag{C 48}$$

so that equation (C 45) can be written

$$(m + 2\rho A^{-1}k^{-2})\,\ddot{V} + sV = 0. \tag{C 49}$$

This defines the local frequency as a function of k (that is, the local dispersion relationship) as

$$\omega = [s/(m + 2\rho A^{-1}k^{-2})]^{\frac{1}{2}}. \tag{C 50}$$

This expression for ω does have the general form (5) predicted in § 7, with a fluid inertia m_f equal to

$$m_f = 2\rho A^{-1}k^{-2}. \tag{C 51}$$

The commentary on figure 4(*b*) discusses at length the physical reason why this fluid inertia has a k^{-2} dependence. (Note also that, for the rectangular scala of height l and breadth $B = 2l$ there assumed, equation (C 51) does become exactly $\rho(kl)^{-2}$.)

It is convenient to solve (C 50) for k as

$$k = k_1\omega(\omega_r^2 - \omega^2)^{-\frac{1}{2}} \quad \text{with} \quad k_1 = (2\rho/Am)^{\frac{1}{2}}. \tag{C 52}$$

Here, k_1 may vary gradually with x while the resonant frequency ω_r varies far more steeply along the cochlea. Equation (C 52) makes the energy propagation velocity (group velocity) equal to

$$U = (\partial k/\partial\omega)^{-1} = k_1^{-1}\omega_r^{-2}(\omega_r^2 - \omega^2)^{\frac{3}{2}}. \tag{C 53}$$

The results (C 52) and (C 53) are fully in agreement with the general theory of appendix B for systems with critical-layer absorption; specifically, they agree with (B 6) and (B 8) for the case $N = \frac{1}{2}$.

The energy per unit length still takes the form (C 5) (twice the potential energy) in terms of the pressure amplitude $f(x)$, but it is now more convenient to write this in terms of the amplitude $|V|$ of the generalized co-ordinate V. The energy per unit length is the average of sV^2 which is

$$\tfrac{1}{2}s|V|^2 = \tfrac{1}{2}m\omega_r^2|V|^2. \tag{C 54}$$

Accordingly, we see that the energy flow rate (U times (C 54)) is

$$\tfrac{1}{2}mk_1^{-1}(\omega_r^2 - \omega^2)^{\frac{3}{2}}|V|^2. \tag{C 55}$$

For waves of fixed frequency ω, then, constant energy flow requires $|V|$ to vary in proportion to

$$(k_1/m)^{\frac{1}{2}}(\omega_r^2-\omega^2)^{-\frac{3}{4}}. \tag{C 56}$$

This shows the expected build-up at the point where the resonant frequency ω_r is equal to ω.

Further details can be given in a specially simple form in the case (C 13), which by (C 46) makes ω_r proportional to $\exp(-\alpha x)$ with A constant, provided that the partition inertia m is also taken constant. This is the interesting case for which Schroeder (1973) and Zweig (1976) worked out the WKB solution in some detail, and verified that it had properties broadly similar to those observed by Rhode (1971). The solution in question is also of rather more general value as an indication of *local* behaviour in any region near enough to a point of resonance for A and m to vary insignificantly within the region.

In this case, the phase θ takes the form

$$\theta = \alpha^{-1}k_1 \tan^{-1}[(\omega_r^2-\omega^2)^{\frac{1}{2}}\omega^{-1}] + \text{constant}, \tag{C 57}$$

as may be verified by differentiating (C 57) to show from (C 52) that $k = -\partial\theta/\partial x$. Expression (C 57) for phase shows the expected tendency to fall with increasing steepness as the point with $\omega_r = \omega$ is approached.

Again, for waves of fixed frequency ω, the time taken for wave energy to reach a given point has the form

$$t = \alpha^{-1}k_1(\omega_r^2-\omega^2)^{-\frac{1}{2}} + \text{constant}, \tag{C 58}$$

as may be verified by differentiating (C 58) to show from (C 53) that $\partial t/\partial x = U^{-1}$. (In both the above differentiations, the property $\partial\omega_r/\partial x = -\alpha\omega_r$ of the exponential distribution of resonant frequency is used.)

Equation (C 58) exhibits the fundamental property of *critical-layer absorption*: the time taken to reach the point where $\omega_r = \omega$ is infinite. This allows an unlimited time for any damping, however light, to dissipate all the energy.

The above results confirm that one-dimensional models taking into account partition inertia can exhibit critical-layer absorption. Indeed, as discussed in § 6, this is the secret of their success. The detailed results for such models that are derived above may be borne in mind for comparison with corresponding results for multi-dimensional models to be given in appendices D and E.

Appendix D. Two-dimensional models

The broad success of certain types of one-dimensional model derives, as appendix C has made clear, from their incorporation of critical-layer absorption. On the other hand, their value in certain matters of detail remains uncertain, because of their questionable assumption of one-dimensional motions, associated with a fluid pressure distribution that is uniform over each scala. This appendix is devoted to a preliminary testing of the conditions under which that assumption may or may not be a good approximation.

The testing must be described as preliminary in that this appendix extends the modelling only to *two* dimensions. Specifically, it allows only for a possible variability of the fluid pressure distribution with distance from the cochlear partition. For a

fuller three-dimensional analysis, allowing also for variability across the width of the partition, see appendix E.

In a two-dimensional analysis, the influence of the *height* l of a scala is crucial. Here, l is the distance from the cochlear partition of the opposing rigid boundary provided by the temporal bone. In terms of this height l, the assumptions of a one-dimensional theory are shown to break down when kl is large enough (where k is the wavenumber).

Of course, a real cochlear cross-section is practically circular, so that the height l, as just defined, is hardly a precise constant. A pure two-dimensional model cannot allow, however, for variation of l (or of anything else) across the width of the cochlear partition. Thus, it is limited to the use of a single average value for l. This is equivalent to representing the cochlea's practically circular cross-section by a square (of side $2l$) of the same area. Maintaining the area unaltered ensures that, where the one-dimensional theory (which depends *only* on the area A of a cross-section, and not on other features of its geometry) is valid, its conclusions are unaltered. For a human cochlea, l needs to be taken as around 0·7 mm to make the square of side $2l$ have the correct cross-sectional area of around 2 mm^2.

The basic characteristic of multi-dimensional models, derived in appendix A (see equation (A 14)), and used also by all other writers, is that the slow-wave pressures p satisfy the fundamental equation for motions of an incompressible fluid: Laplace's equation, $\nabla^2 p = 0$. For two-dimensional models, however, p depends only on distance x along the cochlea and on distance z from the cochlear partition, so that this equation becomes simply

$$\partial^2 p/\partial x^2 + \partial^2 p/\partial z^2 = 0. \tag{D 1}$$

If now we make the WKB approximation then, as explained in appendix C following equation (C 47), we must move towards a dispersion relationship through a process in which each $(\partial/\partial x)$ is replaced by $(-ik)$. Equation (D 1) then becomes

$$\partial^2 p/\partial z^2 - k^2 p = 0, \tag{D 2}$$

an equation of which the general solution takes the form

$$p = p_+ e^{kz} + p_- e^{-kz}, \tag{D 3}$$

with p_+ and p_- constant. Now, at the assumed distance $z = l$ from the cochlear partition, the rigid boundary makes any acceleration perpendicular to it impossible, so that the pressure gradient $\partial p/\partial z$ must be zero. This gives

$$kp_+ e^{kl} - kp_- e^{-kl} = 0. \tag{D 4}$$

Equations (D 3) and (D 4) can be used to relate the generalized co-ordinate V, that was introduced in appendix C to describe the motion of the cochlear partition, to the local value of the pressure fluctuation p. Such a relationship can be used in combination with the equation of motion (C 45) of the partition itself to define a dispersion relationship.

Since, in our two-dimensional model, the definition of the generalized co-ordinate makes its second time derivative $\ddot{V}$ equal to the width $2l$ of the cochlear partition multiplied by the *acceleration* of the adjacent fluid, which in turn is generated by pressure gradient, we have

$$\rho \ddot{V} = 2l(\partial p/\partial z)_{z=0} = 2kl(p_+ - p_-). \tag{D 5}$$

Also, the local pressure fluctuation p at the cochlear partition is

$$(p)_{z=0} = p_+ + p_-. \tag{D 6}$$

Here, by (D 4), $p_- = p_+ e^{2kl}$, so that (D 5) and (D 6) give

$$(2p)_{z=0} = -\rho \ddot{V} I(kl), \quad \text{where} \quad I(kl) = (e^{2kl}+1)/[kl(e^{2kl}-1)]. \tag{D 7}$$

It is this local value (D 7) of the pressure difference across the cochlear partition that forces its motion in accordance with equation (C 45). We now see, by (D 7), that this equation of motion can be written

$$(m+m_f)\,\ddot{V} + sV = 0, \tag{D 8}$$

where the effective fluid inertia m_f is

$$m_f = \rho I(kl) = \rho(kl)^{-1}[(e^{2kl}+1)/(e^{2kl}-1)]. \tag{D 9}$$

It is the non-dimensional quantity $m_f/\rho = I(kl)$ which is plotted in figure 3. Note that it coincides with the one-dimensional value $(kl)^{-2}$ given by (C 51) for small enough kl. However, for $kl > 0{\cdot}5$ it already deviates significantly from that value given by one-dimensional theory. With $l = 0{\cdot}7$ mm, this *condition for one-dimensional theory to become inadequate* is $k > 0{\cdot}7$ mm^{-1}.

At still larger values of kl (say, $kl > 1{\cdot}5$, corresponding to $k > 2$ mm^{-1}) the expression in square brackets in (D 9) is very close to 1, so that effectively we have

$$m_f = \rho(kl)^{-1}. \tag{D 10}$$

This is the limit in which, by (D 4), p_+ becomes insignificant compared with p_- so that the fluid motions fall off like e^{-kz} with distance from the partition. Then, as k increases, the fluid motion becomes effectively confined within a smaller and smaller distance, of order k^{-1}, from the partition; (D 10) represents the decreasing inertia of that narrowing fluid layer. For other aspects of the transition between $\rho(kl)^{-2}$ for small kl and $\rho(kl)^{-1}$ for large kl, see the discussion centred upon figure 4.

The basic dispersion relationship (5) relating frequency to the sum of partition inertia and fluid inertia takes a specially interesting form in the case (D 10) which applies for $k > 2$ mm^{-1}. This form comes within the general analysis of critical-layer absorption given at the end of appendix B, but it corresponds to a value $N = 1$ as opposed to the value $N = \frac{1}{2}$ noted in appendix C as found when the same phenomena are analysed on the over-simplified one-dimensional theory.

Solving the dispersion relationship

$$\omega = \{s/[m+\rho(kl)^{-1}]\}^{\frac{1}{2}} \tag{D 11}$$

for k, where $\omega_r = (s/m)^{\frac{1}{2}}$, we obtain

$$kl = \rho m^{-1}\omega^2(\omega_r^2 - \omega^2)^{-1}. \tag{D 12}$$

The corresponding energy propagation velocity (group velocity) is

$$U = (\partial k/\partial\omega)^{-1} = ml\rho^{-1}(2\omega\omega_r^2)^{-1}(\omega_r^2-\omega^2)^2. \tag{D 13}$$

Continuing to write the energy per unit length in the form (C 54), we multiply this by U to obtain the energy flow as

$$\tfrac{1}{4}m^2 l\rho^{-1}\omega^{-1}(\omega_r^2-\omega^2)^2\,|V|^2. \tag{D 14}$$

For waves of fixed frequency, then, constant energy flow requires the amplitude $|V|$ to vary in proportion to

$$m^{-1}l^{-\frac{1}{2}}(\omega_r^2-\omega^2)^{-1}. \tag{D 15}$$

This is an only slightly more rapid build-up towards the point of resonance that is indicated (equation (C 56)) on one-dimensional theory.

As in appendix C, we can give further details in a specially simple form in the case (C 13) with ω_r proportional to $\exp(-\alpha x)$ and with l constant (since $A = 2l^2$ is to be constant). In this case, the phase θ has the form

$$\theta = (\rho/2\alpha lm)\ln(1-\omega^2\omega_r^{-2}) + \text{constant}, \tag{D 16}$$

as may be verified by differentiating (D 16) to show from (D 12) that $\partial\theta/\partial x = -k$. Equation (D 16) shows a still more pronounced tendency than does (C 57) for the phase to fall with increasing steepness as the point with $\omega_r = \omega$ is approached.

Again, for waves of fixed frequency ω, the time taken for wave energy to reach a given point is

$$t = (\rho/\alpha lm)\,\omega(\omega_r^2-\omega^2)^{-1}, \tag{D 17}$$

as may be verified by differentiating (D 17) to show from (D 13) that $\partial t/\partial x = U^{-1}$. Equation (D 17) shows that the most important property of critical-layer absorption (unlimited time available for damping of wave energy ahead of the point of resonance) is present to an even more marked degree for two-dimensional models than is indicated by (C 58) for one-dimensional models.

The general behaviour near the point of resonance indicated by (D 12), (D 15), (D 16) and (D 17) is important because it will be found in appendix E to be retained for the much more realistic three-dimensional models with critical-layer absorption. The results were set out graphically in figure 6. Here, the graph marked (*a*) represents expression (6), to which are proportional *both* (i), by (D 12), the wavenumber k; *and* (ii), by (D 17), the time $(\omega t/2\pi)$, measured in wave periods, required for wave energy to reach a point. Similarly, graph (*b*) represents expression (7), which by (D 16) is proportional to phase.

Finally, graph (*c*) represents an 'amplitude intensification factor' $|V|/|V_1|$, where $|V_1|$ is amplitude given, on the WKB approximation, by a stiffness-dominated one-dimensional model. On such a model, the energy propagation velocity is the slow-wave speed c, which by (C 39) with $A = 2l^2$ can be written

$$c = l(s/\rho)^{\frac{1}{2}} = l(m/\rho)^{\frac{1}{2}}\omega_r. \tag{D 18}$$

Multiplying this by (C 54) we obtain the energy flow for waves of amplitude $|V_1|$ as

$$\tfrac{1}{2}ml(m/\rho)^{\frac{1}{2}}\omega_r^3|V_1|^2. \tag{D 19}$$

Equating this to (D 14) we obtain the amplitude intensification factor (that is, the ratio $|V|/|V_1|$ for fixed energy flow) as

$$\frac{|V|}{|V_1|} = \left(\frac{4\rho}{m}\right)^{\frac{1}{4}}\left[\frac{(\omega/\omega_r)^{\frac{1}{2}}}{1-(\omega/\omega_r)^2}\right]. \tag{D 20}$$

Here, the quantity in square brackets is given in § 10 as expression (8), and plotted on a decibel scale in figure 6 as graph (*c*).

Appendix E. Three-dimensional models

Any balance-sheet of the merits and demerits, as realistic descriptions of cochlear mechanics, exhibited by models that are one-dimensional (appendix C) or two-dimensional (appendix D) must be very evenly divided between them. There is one respect in which two-dimensional models are greatly superior: at relatively higher wavenumbers ($k > 0{\cdot}7$ mm^{-1}) they make due allowance for variability of fluid motions with distance from the cochlear partition; while, especially, at wavenumbers exceeding about 2 mm^{-1}, they allow for those motions to be confined within a narrow layer whose thickness decreases like k^{-1} as k increases. No such variability is allowed for in one-dimensional models.

On the other hand, two-dimensional models are grossly unrealistic in that they allow for no variation at all across the *width* of the cochlear partition. In this matter, a one-dimensional model is greatly superior, allowing as in (C 40) for a realistic shape of bending mode of the partition. Two-dimensional models presuppose the absurdly unrealistic bending mode in which $\zeta(y) =$ constant; as if the bony shelf *and* all parts of the basilar membrane *and* the spiral ligament could all make uniformly equal transverse displacements. . . . .

There is one other feature of two-dimensional models which may, possibly, appear unsatisfactory from the standpoint of biological realism; but which, nevertheless, must be regarded as unlikely to degrade significantly those models' representations of cochlear mechanics. This is the replacement of the cochlea's practically circular cross-section by a square of the same area. This change, however repugnant it might seem, cannot substantially reduce the accuracy of two-dimensional models, because (i) for the lower values of kl they become identical with one-dimensional models, whose properties depend *only* on the area and not on the shape of a cross-section; while (ii) for the larger values of kl the fluid motions are progressively confined more and more to the neighbourhood of the cochlear partition, where they cannot be significantly influenced by the shape of the rigid boundary. To sum up, the grossly unrealistic feature in two-dimensional models is the neglect of variability of bending displacement across the cochlear partition's width, and *not* any neglect of the corresponding variability in the height of a scala.

Only a proper three-dimensional model, such as Steele (1974) pioneered, can avoid the principal demerits of both the one-dimensional and the two-dimensional models. A three-dimensional model can readily allow for a fully realistic shape (C 40) of bending mode of the cochlear partition across its width. At the same time, it can take full account of the variability of fluid motions with distance from the partition. The mathematics, however, is greatly simplified if we continue to represent the cochlear cross-section as a square of side $2l$; a simplification which, for the reasons just given, may be adopted with some confidence.

The mathematical simplification just mentioned results entirely from the fact that, in a square cross-section, the pressure distribution can be conveniently expanded in a Fourier series,

$$p = p_0(x,z) + 2\sum_{n=1}^{\infty} p_n(x,z)\cos(n\pi y/2l) \qquad \text{(E 1)}$$

for $0 < y < 2l$. This series comprises cosines only (and not sines) because the pressure gradient $\partial p/\partial y$ must be zero at $y = 0$ and $y = 2l$ (which, as rigid boundaries, neces-

sarily prevent any fluid accelerations perpendicular to them). Because every term in (E 1) must separately satisfy Laplace's equation, the coefficient $p_n(x, z)$ has to satisfy

$$\partial^2 p_n/\partial x^2 + \partial^2 p_n/\partial z^2 - (n\pi/2l)^2 p_n = 0. \tag{E 2}$$

This coincides with (D 1) only in the case $n = 0$.

If now we make the WKB approximation then, as explained in appendix C following equation (C 47), we must move towards a dispersion relationship through a process in which each $(\partial/\partial x)$ is replaced by $(-ik)$. Equation (E 2) then becomes

$$\partial^2 p_n/\partial z^2 - [k^2 + (n\pi/2l)^2] p_n = 0. \tag{E 3}$$

We may conveniently note that this is identical with the corresponding two-dimensional equation (D 2) for p with

$$k \quad \text{replaced by} \quad [k^2 + (n\pi/2l)^2]^{\frac{1}{2}}; \tag{E 4}$$

a rather simple substitution.

It is straightforward to relate the above Fourier series for pressure to a fully realistic shape (C 40) of bending mode in terms of the values of the integrals

$$\zeta_n = \int_0^{2l} \zeta(y) \cos(n\pi y/2l)\, dy \tag{E 5}$$

calculated for that mode. Each integral (E 5) is a non-dimensional quantity; and, indeed, by (C 43), ζ_0 has the value 1. Furthermore, the Fourier series representation of the boundary displacement $V\zeta(y)$ has the form

$$V\zeta(y) = V(2l)^{-1}\left[\zeta_0 + 2\sum_{n=1}^{\infty} \zeta_n \cos(n\pi y/2l)\right]. \tag{E 6}$$

The pressure gradient $(\partial p/\partial z)$ at the cochlear partition must be equal to the density ρ times the *local acceleration*, which is the second time derivative $\ddot{V}\zeta(y)$ of (E 6). By (E 1), this gives a boundary condition

$$\rho \ddot{V}\zeta_n = 2l(\partial p_n/\partial z)_{z=0}, \tag{E 7}$$

which is identical with (D 5) except for the additional non-dimensional factor ζ_n on the left-hand side. The corresponding condition at the rigid boundary $z = l$ is, on the other hand, unchanged:

$$(\partial p_n/\partial z)_{z=l} = 0. \tag{E 8}$$

There is absolutely no need to repeat the mathematics of solving (E 3) subject to (E 7) and (E 8) and deducing $(2p_n)_{z=0}$. That mathematics was given in appendix D (equations (D 3) to (D 7)) and remains the same except for (i) the substitution (E 4) and (ii) the extra factor on the left of (E 7). Accordingly, the solution is

$$(2p_n)_{z=0} = -\rho \ddot{V}\zeta_n I([k^2 l^2 + \tfrac{1}{4}n^2\pi^2]^{\frac{1}{2}}) \tag{E 9}$$

where the function I is defined in (D 7) and plotted in figure 3. Substituted in (E 1), this gives the Fourier series for the pressure difference $(2p)_{z=0}$ which forces the motions of the cochlear partition.

When this pressure difference varies with y, the right-hand side of the energy equation (C 44) is modified to

$$\int_0^{2l} (2p)_{z=0} [\dot{V}\zeta(y)]\, dy, \tag{E 10}$$

representing the rate of working by the distributed pressure difference $(2p)_{z=0}$ in the actual bending mode (C 40). By (E 1) and (E 5) this rate of working is

$$\dot{V}\left[(2p_0)_{z=0} + 2\sum_{n=1}^{\infty} (2p_n)_{z=0}\,\zeta_n\right]. \tag{E 11}$$

With the right-hand side of (C 44) replaced by (E 11) we obtain, on division by $\dot{V}$, the equation of motion

$$m\ddot{V} + sV = (2p_0)_{z=0} + 2\sum_{n=1}^{\infty} (2p_n)_{z=0}\,\zeta_n \tag{E 12}$$

for the cochlear partition. This determines at once the fluid inertia m_f since, by (E 9), equation (E 12) taken the form $(m+m_f)\ddot{V} + sV = 0$ with

$$m_f/\rho = I(kl) + 2\sum_{n=1}^{\infty} \zeta_n^2 I([k^2l^2 + \tfrac{1}{4}n^2\pi^2]^{-\frac{1}{2}}). \tag{E 13}$$

Equation (E 13) is a relatively simple form for the fluid inertia in terms of the constants (E 5) for the bending mode and the function I defined in (D 7) and plotted in figure 3.

The above calculation of m_f, on a three-dimensional model that avoids the main deficiencies of both the one-dimensional and two-dimensional models, answers at once the question: 'which of those two models gives better results?' The answer is: 'the two-dimensional model'; for such a model gives m_f/ρ a value $I(kl)$ *larger* than the corresponding one-dimensional value $(kl)^{-2}$ whereas the more accurate result (E 13) makes m_f/ρ larger still; also, the ratio of the more accurate result (E 13) to $I(kl)$ can never exceed the finite upper bound

$$1 + 2\sum_{n=1}^{\infty} \zeta_n^2 = 2l\int_0^{2l} [\zeta(y)]^2\, dy, \tag{E 14}$$

whereas the ratio of $I(kl)$ to the one-dimensional value $(kl)^{-2}$ grows without limit as kl increases. If anything, the incorporation of three-dimensional effects intensifies the distinction noted already (appendix D) between two-dimensional and one-dimensional models, because the decrease of fluid inertia with increasing kl is made a little more gradual still, so as to retard energy flow still more steeply and enhance critical-layer absorption.

On the whole, however, the principal conclusion from (E 13) is the quite modest quantitative extent of the change from two-dimensional theory. For moderate values of kl the ratio of (E 13) to $I(kl)$ is even less than its upper bound (E 14); a bound which should be attained only when kl is so large that $I([k^2l^2 + \frac{1}{4}n^2\pi^2]^{\frac{1}{2}})$ is indistinguishable from $I(kl)$ for all those values of n for which J_n is significant. From a qualitative standpoint, (E 13) implies that we are dealing with critical-layer absorption of the general type described in appendix B (equation (B 6) onwards) with $N = 1$; accordingly, the local behaviour near the point of resonance is as calculated in appendix D and plotted in figure 6.

For practical purposes, (E 13) can be simplified to

$$m_f/\rho = I(kl) + 2\sum_{n=1}^{\infty} \zeta_n^2 (k^2l^2 + \tfrac{1}{4}n^2\pi^2)^{-\frac{1}{2}} \qquad \text{(E 15)}$$

since figure 3 shows $I(x)$ to be practically indistinguishable from x^{-1} for $x > \frac{1}{2}\pi$ (it is at most in the term $n = 1$ that (E 15) might differ noticeably from (E 13), but equation (E 5) for ζ_n makes ζ_1^2 very small because $\cos(\pi y/2l)$ becomes zero within the main region of partition displacement). Expression (E 15) is easy to compute for various assumed bending modes of the cochlear partition.

One great advantage of the WKB method is that it can be readily applied so as to take into account those gradual variations in the geometry of the cochlear partition that occur along the length of the cochlea. Prominent among these is the gradual increase in the breadth, $2b$, of the basilar membrane with distance from the base, which occurs even while the overall width, $2l$, of the cochlea is becoming less. There is, in consequence, a quite significant gradual increase in the proportion b/l of the whole width of the cochlear partition taken up by basilar membrane.

All this can be allowed for in the WKB method: the gradual changes in b/l produce similar gradual changes in the constants ζ_n and so in the fluid inertia (E 15). At each point, the dispersion relationship

$$\omega = [s/(m + m_f)]^{\frac{1}{2}} \qquad \text{(E 16)}$$

leads to an expression for the energy propagation velocity, $U = \partial\omega/\partial k$, associated with the waves of a given frequency, in terms of which their amplitude distribution can be derived from constancy of energy flow.

One simple calculation, as follows, can illustrate *both* the relatively modest extent of the change from two-dimensional theory *and* the fact that this change varies with b/l in a manner that is straightforward to compute for any particular model of cochlear-partition bending. In the calculation which follows, the mid-points of the cochlear partition and of the basilar membrane are taken to coincide at $y = l$. Furthermore, a simple model of basilar-membrane deflection is adopted; essentially, 'Model 1' of Steele (1974). In the context of the present paper, there is no point in pursuing more sophisticated bending-mode models because Steele and his associates have covered this ground rather thoroughly; the effect in each case is to produce a slightly different dependence of the constants ζ_n on b/l and, thus, to modify the way in which m_f, in the dispersion relationship (E 16), varies with b/l as well as with kl.

The simple bending mode assumed here is a half-wavelength sine wave confined to the basilar membrane alone. Thus,

$$\zeta(y) = (\pi/4b)\cos[\pi(y-l)/2b] \quad \text{for} \quad |y-l| < b; \quad \zeta(y) = 0 \quad \text{for} \quad |y-l| > b; \quad \text{(E 17)}$$

which, essentially, is the shape of the principal bending mode if the basilar membrane is taken as 'simply supported' at rigid supports. A mode like (E 17) with discontinuities of *slope* at $y = l \pm b$ may give quite a stringent test of how far three-dimensional theory may depart from two-dimensional theory, because it makes the constants ζ_n fall off only in proportion to n^{-2} for large n (as opposed to n^{-3} for a mode without discontinuities of slope).

Actually, for the mode (E 17) the constant ζ_n takes the value

$$\zeta_n = \{[1-(nb/l)^2]^{-1}\cos(\tfrac{1}{2}n\pi b/l)\}\cos(\tfrac{1}{2}n\pi). \qquad \text{(E 18)}$$

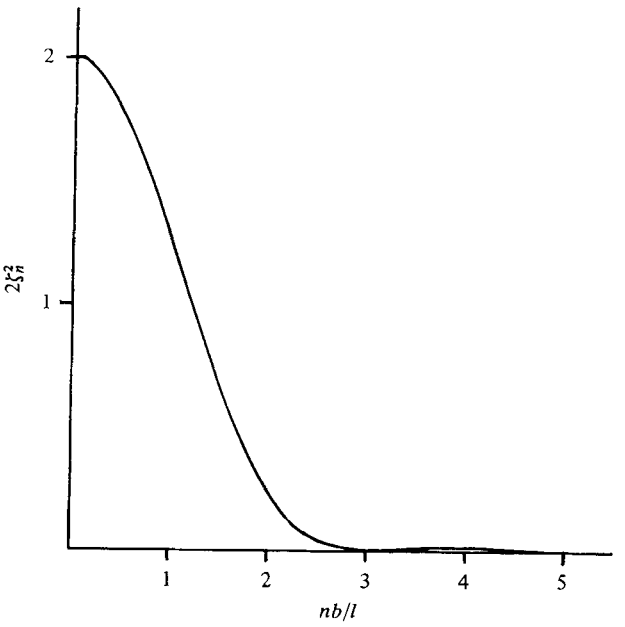

FIGURE 16. When n is even, the coefficients $2\zeta_n^2$ occurring in equations (E 13) and (E 15) take, for the bending mode (E 17), the values shown (plotted as a function of nb/l). When n is odd, $\zeta_n = 0$.

Here, the last factor $\cos(\frac{1}{2}n\pi)$ simply reflects a property of any *symmetrical* bending mode, that ζ_n is zero whenever n is odd. The remaining factor (in curly brackets) is a function of nb/l alone; which, in the only case ($nb/l = 1$) where it appears to be undefined, is to be replaced by its limiting value $\frac{1}{4}\pi$. Figure 16 uses (E 18) to plot as a function of nb/l the values of the important coefficient $2\zeta_n^2$ which occurs in (E 13) or (E 15) *when n is even only* (it is zero when n is odd). In spite of the point made in the preceding paragraph, this coefficient becomes quite insignificant for $nb/l \geqslant 3$. For most practical values of b/l, therefore, the number of terms making a significant contribution in (E 15) is quite modest.

Figure 17 uses these results to plot five different values for the fluid inertia m_f. Thus, it gives a log–log plot of m_f/ρ against kl as calculated from one-dimensional theory (dotted line marked 1D), two-dimensional theory (2D) and three cases (3D) of three-dimensional theory. These are cases corresponding to cochlear cross-sections where the ratio b/l between the breadths of the basilar membrane and of the whole cochlear partition takes values 0·25, 0·5 and 0·75. The broken lines represent in each case the upper bound set by expression (E 14) to the ratio of m_f/ρ to $I(kl)$.

The important property of the 3D curves in figure 17 from the standpoint of critical-layer absorption is exhibited in the lower part of the diagram. This is the part relevant to the general neighbourhood of a point of resonance; more precisely, it is the part where m_f/ρ is falling towards low values, which may be even less than the corresponding values m/ρ for the inertia of the cochlear partition. In this part of the diagram, the dependence of m_f/ρ on kl is tending rapidly towards the same 45° slope for the 3D curves as for the 2D curve; in other words, towards the same variation as $(kl)^{-1}$.

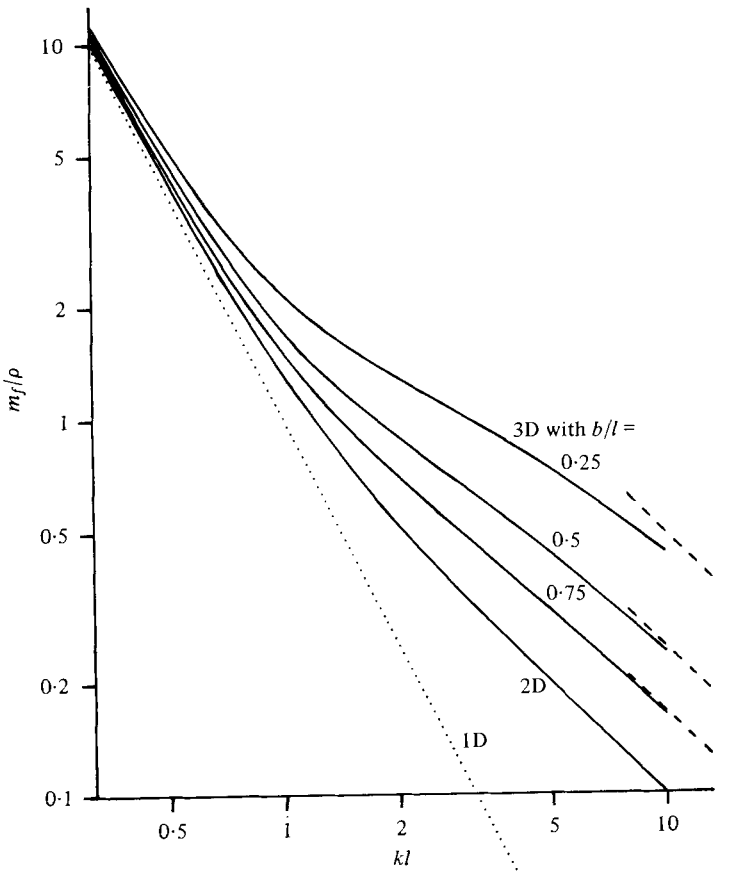

FIGURE 17. The ratio m_f/ρ of fluid inertia to density, shown on a log–log plot against kl for the bending mode (E 17) with b/l = 0·25, 0·5 and 0·75. Results on the one- and two-dimensional theories of appendices C and D (as previously given on a linear plot in figure 3) are included for comparison.

This is the type of variation that led to the results plotted in figure 6; results which, as we now see, may be used near the point of resonance even on the basis of three-dimensional theory.

In addition, the upper part of figure 17 gives some new and definitely interesting information. This is the part where the m term in the dispersion relationship (E 16) may be negligible, so that at the cross-section in question ω varies as $m_f^{-\frac{1}{2}}$.

Essentially, this upper part of the diagram predicts, especially in regions near the base where b/l is relatively small, *a much greater degree of dispersion* for $kl > 0{\cdot}5$ (that is, for $k > 0{\cdot}7$ mm^{-1}) than would be predicted on two-dimensional theory. In this region the 1D curve represents absence of dispersion (m_f proportional to k^{-2} makes ω proportional to k). The curve showing the greatest departure from that (and, therefore, the greatest dispersion) is the 3D curve for $b/l = 0{\cdot}25$. Its downward slope is reduced from 2·0 to 0·6 on the log–log plot before rising again to 1·0. In the region around $kl = 1{\cdot}5$ (that is, $k = 2$ mm^{-1}) where that downward slope is 0·6 the resulting frequency ω is proportional to $k^{0{\cdot}3}$ (compare $k^{0{\cdot}5}$ on two-dimensional theory).

Accordingly, the energy propagation velocity $\partial\omega/\partial k$ has fallen, not just to 0·5 times, but to 0·3 times the velocity of wave crests. This effect may assist the all-important process of reduction in the speed of energy propagation to make a somewhat earlier start.†

In short, three-dimensional models permit an anticipatory slowing down of energy propagation to precede its final bringing to a halt at the point of resonance. This property, like many of the others noted in appendix E, has also been emphasized by Steele & Taber (1979*b*).

REFERENCES

ALLEN, J. B. 1977 Two-dimensional cochlear fluid model: new results. *J. Acoust. Soc. Am.* **61**, 110–119.

BÉKÉSY, G. VON 1941 Über die Elastizität der Schneckentrennwand des Ohres. *Akust. Zeits.* **6**, 265–278.

BÉKÉSY, G. VON 1947 The variation of phase along the basilar membrane with sinusoidal vibrations. *J. Acoust. Soc. Am.* **19**, 452–460.

BÉKÉSY, G. VON 1960 *Experiments in Hearing.* McGraw-Hill.

BERKLEY, D. A. & LESSER, M. B. 1973 Comparison of single- and double-chamber models of the cochlea. *J. Acoust. Soc. Am.* **53**, 1037–1038.

BOER, E. DE 1979 Short-wave world revisited: resonance in a two-dimensional cochlear model. *Hearing Res.* **1**, 253–258.

BOGERT, B. P. 1950 Determination of the effects of dissipation in the cochlear partition by means of a network representing the basilar membrane. *J. Acoust. Soc. Am.* **23**, 151–154.

BOOKER, J. R. & BRETHERTON, F. P. 1967 The critical layer for internal gravity waves in a shear flow. *J. Fluid Mech.* **27**, 513–539.

COLE, J. D. & CHADWICK, R. S. 1977 An approach to the mechanics of the cochlea. *Z. angew. Math. Phys.* **28**, 785–804.

EVANS, E. F. & WILSON, J. P. 1973 The frequency selectivity of the cochlea. In *Basic Mechanisms in Hearing* (ed. A. R. Møller), pp. 519–554. Academic.

FETTIPLACE, R. & CRAWFORD, A. C. 1978 The coding of sound pressure and frequency in cochlear hair cells of the terrapin. *Proc. Roy. Soc.* B **203**, 209–218.

FLETCHER, H. 1951 On the dynamics of the cochlea. *J. Acoust. Soc. Am.* **23**, 637–645.

GEISLER, C. D. 1976 Mathematical models of the mechanics of the inner ear. In *Handbook of Sensory Physiology*, vol. v/3. *Auditory System: Clinical and Special Topics* (ed. W. D. Keidel & W. D. Neff), pp. 391–415. Springer.

GREENWOOD, D. D. 1961 Critical bandwidth and the frequency co-ordinates of the basilar membrane. *J. Acoust. Soc. Am.* **33**, 1344–1357.

GUNDERSEN, T., SKARSTEIN, Ø. & SIKKELAND, T. 1978 A study of the vibration of the basilar membrane in human temporal bone preparations by the use of the Mössbauer effect. *Acta Otolaryngol.* **86**, 225–232.

HUXLEY, A. F. 1969 Is resonance possible in the cochlea after all? *Nature* **221**, 935–940.

JOHNSTONE, B. M., TAYLOR, K. J. & BOYLE, A. J. 1970 Mechanics of the guinea pig cochlea. *J. Acoust. Soc. Am.* **47**, 504–509.

KIANG, N. Y. S. & MOXON, E. C. 1974 Tails of tuning curves of auditory-nerve fibres. *J. Acoust. Soc. Am.* **55**, 620–630.

KIANG, N. Y. S., WATANABE, T., THOMAS, E. C. & CLARK, L. F. 1965 *Discharge Patterns of Single Fibres in the Cat's Auditory Nerve.* Massachusetts Institute of Technology Press.

KOHLLÖFFEL, W. E. 1972 A study of basilar-membrane vibrations. *Acustica* **27**, 49–89.

† All of the above-noted properties of m_f exhibited in figure 17 must, in general, be found for any assumed bending mode $\zeta(y)$, because they represent necessary mathematical behaviour of a sum such as (E 15) in which only a small number of the coefficients $2\zeta_n^2$ are significant.

KOHLLÖFFEL, W. E. 1973 Observations of the mechanical disturbances along the basilar membrane with laser illumination. In *Basic Mechanisms in Hearing* (ed. A. R. Møller), pp. 95–113. Academic.

LAMING, D. R. J. 1979 Unpublished work, to appear shortly as Chapter 8 of *Weber's Law*. Academic.

LESSER, M. B. & BERKLEY, D. A. 1972 Fluid mechanics of the cochlea, part 1. *J. Fluid Mech.* **51**, 497–512.

LIGHTHILL, J. 1978 *Waves in Fluids*. Cambridge University Press.

PETERSON, L. C. & BOGERT, B. P. 1950 A dynamical theory of the cochlea. *J. Acoust. Soc. Am.* **22**, 369–381.

RANKE, O. F. 1950 Hydrodynamik der Schneckenflüssigkeit. *Zeits. f. Biol.* **103**, 409–434.

RHODE, W. S. 1971 Observation of the vibration of the basilar membrane in squirrel monkeys using the Mössbauer technique. *J. Acoust. Soc. Am.* **49**, 1218–1231.

RHODE, W. S. 1973 An investigation of post-mortem cochlear mechanics using the Mössbauer effect. In *Basic Mechanisms in Hearing* (ed. A. R. Møller), pp. 49–63. Academic.

ROBLES, L., RHODE, W. S. & GEISLER, C. D. 1976 Transient response of the basilar membrane measured in squirrel monkeys using the Mössbauer effect. *J. Acoust. Soc. Am.* **59**, 926–939.

SCHROEDER, M. R. 1973 An integrable model for the basilar membrane. *J. Acoust. Soc. Am.* **53**, 429–434.

SIEBERT, W. M. 1974 Ranke revisited – a simple short-wave cochlear model. *J. Acoust. Soc. Am.* **56**, 594–600.

STEELE, C. R. 1974 Behaviour of the basilar membrane with pure-tone excitation. *J. Acoust. Soc. Am.* **55**, 148–162.

STEELE, C. R. 1976 Cochlear mechanics. In *Handbook of Sensory Physiology*, vol. v/3, Auditory System: Clinical and Special Topics (ed. W. D. Keidel & W. D. Neff), pp. 443–478. Springer.

STEELE, C. R. & TABER, L. A. 1979*a* Comparison of 'WKB' and finite difference calculations for a two-dimensional cochlear model. *J. Acoust. Soc. Am.* **65**, 1001–1006.

STEELE, C. R. & TABER, L. A. 1979*b* Comparison of WKB calculations and experimental results for three-dimensional cochlear models. *J. Acoust. Soc. Am.* **65**, 1007–1018.

VIERGEVER, M. 1980 *Mechanics of the Inner Ear*. Delft University Press.

VOLDŘICH, L. 1978 Mechanical properties of basilar membrane. *Acta Otolaryngol.* **86**, 331–335.

WEVER, E. G. & LAWRENCE, M. 1954 *Physiological Acoustics*. Princeton University Press.

WILSON, J. P. & JOHNSTONE, J. R. 1975 Basilar membrane and middle-ear vibration in guinea pig measured by capacitance probe. *J. Acoust. Soc. Am.* **57**, 705–723.

ZWEIG, G. 1976 Basilar membrane motion. *Cold Spring Harbor Symposia on Quantit. Biol.* **40**, 619–633.

ZWEIG, G., LIPES, R. & PIERCE, J. R. 1976 The cochlear compromise. *J. Acoust. Soc. Am.* **59**, 975–982.

ZWISLOCKI, J. 1948 Theorie der Schneckenmechanik. *Acta Otolaryngol. Suppl.* **72**.

ZWISLOCKI, J. 1965 Analysis of some auditory characteristics. In *Handbook of Mathematical Psychology* (ed. R. D. Luce, R. R. Bush & E. Galanter), vol. III, pp. 1–97. Wiley.